

A Spectroscopic Survey of WNL Stars in the LMC: General Properties and Binary Status

O. Schnurr^{1,2*†}, A. F. J. Moffat¹, N. St-Louis¹, N. I. Morrell³,
and M. A. Guerrero-Roncel⁴

¹*Dépt. de Physique, Université de Montréal, C. P. 6128, succ. centre-ville, Montréal (Qc) H3C 3J7, and Centre de Recherche en Astrophysique du Québec, Canada*

²*Dept. of Physics and Astronomy, University of Sheffield, Hicks Building Hounsfield Road, Sheffield S3 7RH, United Kingdom*

³*Las Campanas Observatory, Observatories of the Carnegie Institution of Washington, Casilla 601, La Serena, Chile*

⁴*Instituto de Astrofísica de Andalucía, Consejo Superior de Investigaciones Científicas, Apartado Correos 3004, E-18080 Granada, Spain*

Version 16 June 2008

ABSTRACT

We report the results of an intense, spectroscopic survey of all 41 late-type, nitrogen-rich Wolf-Rayet (WR) stars in the Large Magellanic Cloud (LMC) observable with ground-based telescopes. This survey concludes the decade-long effort of the Montréal Massive Star Group to monitor every known WR star in the Magellanic Clouds except for the 6 crowded WNL stars in R136, which will be discussed elsewhere. The focus of our survey was to monitor the so-called WNL stars for radial-velocity (RV) variability in order to identify the short- to intermediate-period ($P \lesssim 200$ days) binaries among them. Our results are in line with results of previous studies of other WR subtypes, and show that the binary frequency among LMC WNL stars is statistically consistent with that of WNL stars in the Milky Way. We have identified four previously unknown binaries, bringing the total number of known WNL binaries in the LMC to nine. Since it is very likely that none but one of the binaries are classical, helium-burning WNL stars, but rather superluminous, hence extremely massive, hydrogen-burning objects, our study has dramatically increased the number of known binaries harbouring such objects, and thus paved the way to determine their masses through model-independent, Keplerian orbits. It is expected that some of the stars in our binaries will be among the most massive known. With the binary status of each WR star now known, we also studied the photometric and X-ray properties of our program stars using archival MACHO photometry as well as *Chandra* and *ROSAT* data. We find that one of our presumably single WNL stars is among the X-ray brightest WR sources known. We also identify a binary candidate from its RV variability and X-ray luminosity which harbours the most luminous WR star known in the Local Group.

Key words: binaries: general – stars: evolution – stars: Wolf-Rayet – Magellanic Clouds

1 INTRODUCTION

The optical spectra of Wolf-Rayet (WR) stars feature broad emission lines from highly-ionized elements. These emission lines arise in a fast, hot, and dense stellar wind which is generally optically thick in the inner part, thereby completely

veiling the hydrostatic photosphere of the WR star. Depending on the elements they show in their optical spectra, WR stars are classified into three different subtypes. If a WR star displays predominantly helium (He) and nitrogen (N), which are formed during hydrogen burning via the CNO cycle, the star is classified as WN; if the WR star displays, in addition to He, predominantly carbon (C) or oxygen (O), which are the products of 3α He burning, it is classified as WC or WO.

Due to their chemical properties, it is now generally accepted that classical WR stars are evolved objects, namely

* Visiting Astronomer at the Complejo Astronómico El Leoncito (CASLEO), the Cerro Tololo Inter-American Observatory (CTIO), the South African Astronomical Observatory (SAAO), and the Mount Stromlo and Siding Spring Observatory (MSSSO)
† E-mail: o.schnurr@sheffield.ac.uk

the almost bare, hydrogen-depleted, helium-burning cores of stars whose initial mass on the main sequence (MS) was, at solar metallicity, above $\sim 25M_{\odot}$, i.e. that started their lives as O stars (Lamers et al. 1991; Maeder & Conti 1994). Thus, the key question of WR-star formation is how a WR-star progenitor loses its outer, H-rich envelope to expose the CNO-enriched, deeper layers, and how WR-star formation depends on ambient metallicity. For single stars, three scenarios have been put forward, depending on the initial mass of the star. Stars with initial masses $25M_{\odot} \lesssim M_i \lesssim 40M_{\odot}$ are expected to become red supergiants (RSGs), as which they experience continuous mass loss through winds. Stars with initial masses $40M_{\odot} \lesssim M_i \lesssim 85M_{\odot}$ are believed to turn into luminous blue variables (LBVs), as which they experience outbursts of violent, eruptive shell-ejections (Humphreys & Davidson 1979, Humphreys & Davidson 1994). Stars with even higher initial masses ($M_i \gtrsim 85M_{\odot}$ at solar metallicity) are believed to reach the WN phase while they are still core-hydrogen burning, and to *directly* evolve into classical, He-burning WR stars (Conti 1976) without going through the LBV phase.

In close binaries, Roche-lobe overflow (RLOF) is suspected to enhance WR-star formation by removing the H-rich envelope of the (more evolved) primary (Kippenhahn & Weigert 1967). Paczyński (1967) was the first to note that a thus stripped He-burning core would very likely resemble a WR star. Since RSGs descend from the initially least massive O stars (see above), it follows that RLOF might thus considerably contribute to the total WR numbers, in particular in low-metallicity environments, where radiatively-driven mass-loss rates are expected to be very low (see Vink et al. 2000; Vink et al. 2001). Indeed, older, non-rotating stellar-evolution models were unable to reproduce the observed WR populations at different Z without either enhancing by a factor of two the then-higher mass-loss rates through stellar winds or increasing the fraction of interacting binaries (Maeder & Meynet 1994). While updated models now include stellar rotation, and much better reproduce the observations without the need of increased binary interaction (Maeder & Meynet 2000), the influence of binarity on WR-star formation remains unclear.

From model calculations, Vanbeveren et al. (1998) found that close O+O binaries with initial periods $P \lesssim 1000$ d cannot escape RLOF if the primary star reaches the RSG stage, resulting in WR+O binaries with post-RLOF periods $\lesssim 200$ d (Wellstein & Langer 1999). Hence, in environments where RLOF is expected to become the increasingly important WR-star formation channel (i.e. at lower ambient Z), the fraction of WR binaries with present-day periods of up to 200 days should be higher. This prediction is accessible to observational tests. For such a study, the Magellanic Clouds are the ideal laboratory: *i*) The distances to both the SMC and the LMC are well established and \sim constant for all stars (e.g. Keller & Wood 2006); *ii*) reddening towards the Clouds is low and fairly constant, contrary to the Galaxy (e.g. Nikolaev et al. 2004), *iii*) the WR populations in both Clouds are nearly complete (e.g. Massey & Duffy 2001, but see Massey et al. 2003), *iv*) the WR population is large enough to allow for reasonable statistics. In total, the LMC harbours 132 WR stars (Breysacher et al. 1999, here-

after BAT99¹), while 12 WR stars are known in the SMC (Massey & Duffy 2001; Massey et al. 2003). To search for binaries, the total sample of 144 stars has been split into three distinct studies: Bartzakos et al. (2001) reported the results on the 25 Magellanic Cloud WC/WO stars, while Foellmi et al. (2003a,b) studied the 71 then-known, early-type WNE (=WN2-WN5) stars, with the exception of the H-rich WNE stars in and around the R136 cluster in the 30 Dor region. The observations of a 72nd WNE star, which was newly discovered by Massey et al. (2003) in the SMC, were reported by Foellmi (2004).

In the present paper, we describe our intense, spectroscopic survey of the remaining 41, late-type WNL (=WN5-11) stars in the LMC. The two WN6 stars in the SMC were already studied by Foellmi et al. (2003a). Our survey includes those WNL stars in the periphery of R136 which could be observed with ground-based telescopes without adaptive optics (AO). For the 6 luminous, WN5-7ha stars in the very core of R136, AO-assisted, near-infrared spectroscopy using VLT/SINFONI was used; those results will be reported elsewhere (Schnurr et al., in preparation). The aim of our study is manifold. First and foremost, we will assess the binary status ($P \lesssim 200$ days) of each of our 41 program stars. This will conclude the decade-long effort of the Montréal Massive Star Group to study spectroscopically the entire WR population in the Magellanic Clouds, and pave the way to obtain a much clearer view of the role binarity plays in the evolution of massive stars at different metallicities. Secondly, binaries identified in this study can be used, in the future, to determine their respective masses by using model-independent, Keplerian orbits. Masses of WR stars are of greatest importance in the context of the calibration of both atmospheric and evolutionary models, in particular for the most massive stars. We have ample reason to believe that at least some H-rich WNL stars in our sample belong to the subgroup of very massive, possibly even the most massive stars known in the Local Group (Rauw et al. 1996; Schweickhardt et al. 1999; Rauw et al. 2004; Bonanos et al. 2004). Thirdly and as a side effect, we will be able to put publicly available, archival X-ray data from *Chandra* and *ROSAT* into context with the binary status of our stars, since massive binaries with colliding stellar winds are known to be strong X-ray emitters.

The paper is organized as follows: In Section 2, we will describe the observations of our program stars. In Section 3, we will briefly describe the data reduction. In Section 4, we will describe in detail how we analysed our spectroscopic and X-ray data and the results we obtained. These results will be discussed in Section 5. Section 6 summarizes and concludes this paper.

2 DATA ACQUISITION

2.1 Spectroscopic Observations

Target stars were selected from *The Fourth Catalogue of Population I Wolf-Rayet Stars in the Large Magellanic*

¹ BAT99 lists 134 WR stars in the LMC, but see Moffat (1991) and Niemela et al. (2001) for the revised non-WR status of BAT99-4 and BAT99-6, respectively.

Table 1. List of our program stars as taken from the BAT99 catalogue. BAT99 numbers as well as cross-identification with the Brey, Radcliffe and/or Melnick numbers are given, together with v magnitudes and spectral types, according to BAT99. Stars without a Brey denomination are those that have been newly included into the BAT99 catalogue.

BAT99	Brey	other	v mag	spectral type
12	10a	...	13.72	O3If*/WN6-A
13	12.89	WN10
16	13	...	12.73	WN8h
22	18	R84	12.09	WN9h
30	24	...	13.40	WN6h
32	26	...	12.72	WN6(h)
33	..	R99	11.54	Ofpe/WN9
44	36	...	13.47	WN8h
45	..	BE294	12.80	WN10h
54	44a	...	14.32	WN9h
55	11.99	WN11h
58	47	...	15.1:	WN6h
68	58	...	14.43	WN5-6
76	64	...	13.46	WN9h
77	65	...	13.34	WN7
79	57	...	13.58	WN7+OB
80	65c	...	13.24	O4If/WN6
83	...	R127	10.5 ^a	Ofpe/WN9
89	71	...	14.28	WN7h
91	73	...	13.98	WN7
92	72	R130	11.51	WN6+B1Ia
93	74a	...	13.83	O3If/WN6
95	80	R135	13.16	WN7h
96	81	Mk53	13.74	WN8(h)
97	...	Mk51	13.77	O3If*/WN7-A
98	79	Mk49	12.96	WN6(h)
99	78	Mk39	12.96	O3If*/WN6-A
100	75	R134	12.85	WN6h
102	87	R140a2	12.99	WN6+O
103	87	R140b	13.01	WN6
104	76	Mk37Wb	14.58	O3If*/WN6-A
105	77	Mk42	12.80	O3If*/WN6-A
107	86	R139	12.12	WNL/Of
113	...	Mk30	13.57	O3If*/WN6-A
114	...	Mk35	13.59	O3If*/WN6-A
116	84	Mk34	13.65	WN5h
118	89	...	11.15	WN6h
119	90	...	12.16	WN6(h)
120	91	...	12.59	WN9h
130	12.82	WN11h
133	12.10	WN11h

^aKnown LBV with large photometric variations, cf. Stahl et al. (1983).

Cloud (BAT99). This catalogue lists 134 WR stars of which 47 fall into the WNL (= WN6-11) class, including the two “slash-star” types O3If/WN6 (supposedly H-burning; Crowther & Bohannan 1997) and Ofpe/WN9 (supposedly linked to the LBV phenomenon; see Stahl et al. 1983; Stahl 1987; Crowther et al. 1995; Nota et al. 1996; Pasquali et al. 1997). 41 of these 47 stars (see Table 1) were observed with conventional spectrographs, and the results of those observations are reported here.

Our observations were organized in three different campaigns or “seasons” between 2001 and 2003 to maximize the time coverage, and were carried out during 13

runs at 6 different, 2m-class, southern telescopes. The following observatories were used: Complejo Astronómico El Leoncito (CASLEO), Argentina; Mount Stromlo Observatory (MSO), Australia; Cerro Tololo Inter-American Observatory (CTIO), Chile; South African Astronomical Observatory (SAAO), South Africa; Siding Spring Observatory, Australia; Las Campanas Observatory (LCO), Chile. In total, 99 nights were allocated, but due to bad weather conditions or technical problems, not all nights were useful. Long-slit spectrographs were used at all telescopes. The exact wavelength coverage of the spectra depended on the respective instrument used, but all sets of data included the wavelength range from 4000 to 5000 Å, thereby comprising the strategic emission lines HeII λ 4686 and NIV λ 4058 (however, see below).

To maximize the flux reaching the detector and thus achieve good S/N, a slit width of 1.5” was used during the first two years, but under the very good seeing conditions on Cerro Tololo during summer, this yielded a relatively large RV scatter; we will come back to this problem later in this paper. Therefore, the slit width was reduced to 1” for the last season (2003/04, only at CTIO). The obtained linear dispersion varied from 0.65 Å/pixel (SSO) to 1.64 Å/pixel (CASLEO), with the 3-pixel spectral (velocity) resolution at 4686 Å ranging from $R \sim 2400$ ($\sim 125\text{kms}^{-1}$) to $R \sim 950$ ($\sim 315\text{kms}^{-1}$). Exposure times were chosen to provide a signal-to-noise ratio (S/N) of ~ 50 -70 per collapsed pixel in the blue continuum around 4500 Å, and were adapted to the respective telescope efficiencies and weather conditions. For our faintest stars, long exposures were broken into two or three to facilitate cosmic-ray rejection.

Even under best conditions, not more than two thirds to three quarters of our sample (“sequence A”) could be observed in one night. The remaining stars (“sequence B”) were then observed the following night before sequence A was restarted again, and so forth. To further break integer-day sampling (~ 2 -day sampling in particular), we also employed a scheme to re-observe the stars of a given sequence the following night before resuming observations of the other sequence, thereby obtaining a ~ 1 -day sampling (i.e. observations were carried out as ABBAABAB etc.). At CTIO, where we had relatively long runs of clear contiguous nights so that we could sufficiently plan ahead, this was particularly successfully employed. Moreover, some stars were observed more frequently (i.e. once or twice every night) by default because they were of particular interest (short-period and/or supposedly very massive binaries).

At the beginning of each night, bias frames and high-S/N, internal (Quartz lamp) flatfield frames were taken. For reliable RVs, a comparison-arc exposure was taken before and after each science exposure, the exception to this rule being the stars in the periphery of R136, because telescope slews were only very minor ($\lesssim 1'$) and differential flexure of the Cassegrain spectrographs not an issue. Neither dark nor twilight-flatfield frames were taken.

The observation journal is summarized in Table 2, while the instrumental properties are summarized in Table 3.

Table 2. Journal of observations.

Run#	Observatory	Start (UT)	End (UT)	Clear nights	Season
1	CASLEO	02 Nov 2001	09 Nov 2001	6	1
2	MSO	09 Nov 2001	06 Dec 2001	14	1
3	CTIO	26 Dec 2001	31 Dec 2001	6	1
4	CTIO	23 Jan 2002	27 Jan 2002	4	1
5	SAAO	05 Nov 2002	12 Nov 2002	7	2
6	CTIO	19 Nov 2002	27 Nov 2002	8	2
7	CTIO	16 Dec 2002	24 Dec 2002	8	2
8	MSO	03 Jan 2003	18 Jan 2003	10	2
9	SSO	27 Jan 2003	31 Jan 2003	3	2
10	LCO	27 Jan 2003	02 Feb 2003	6	2
11	CTIO	19 Dec 2003	29 Dec 2003	10	3
12	CTIO	02 Jan 2004	06 Jan 2004	4	3
13	CTIO	07 Jan 2004	09 Jan 2004	2	3

Table 3. List of observatories and instruments used.

Observatory	CASLEO	MSO	CTIO	SAAO	SSO	LCO
Telescope	2.15m	1.88m	1.5m	1.88m	2.3m	2.5m
Spectrograph	REOSC	CassSpec	RCSpec	GratingSpec	DBS ^a	WFCCD
Grating [l/mm]	600	600	600	600	600	600
Dispersion [$\text{\AA}/\text{pix}$]	1.64	1.35	1.48	1.10	0.65	1.38
R @ 4686 \AA (3 pixels)	945	1160	1055	1420	2400	1130
Spectral range [\AA]	3970-5645	3885-5515	3980-5730	3485-5415	3905-4875	3775-5600
Comparison lamp	HeNeAr	FeAr	HeNeAr	CuAr	CuHeAr	HeH
Overscan	no	no	yes	yes	yes	yes

Notes: ^aBlue arm only.

2.2 Archival X-ray Data

We made use of public archives to retrieve X-ray data for our program stars. The *Chandra* Archive² available from October 2004 and the entire *ROSAT* Archive³ have been searched for all *Chandra* ACIS and *ROSAT* PSPC and HRI observations including any of the 41 WNL stars studied in this paper. We de-archived *Chandra* ACIS observations for 25 WNL stars, and *ROSAT* PSPC and HRI observations for 13 and 3 WNL stars, respectively. A summarizing table of these observations is provided in Section 4.8 (Table 13). Further details of the selection and reduction of these observations are provided by Guerrero & Chu (2006).

2.3 Archival photometry

Several microlensing surveys carry out repeated photometry towards the LMC and make their data publicly available. In order to obtain repeated photometry of our program stars, we thus browsed through the public archives of the Massive Compact Halo Object (MACHO; see Alcock et al. 1996) experiment, and the Optical Gravitational Lensing Experiment (OGLE; see Udalski et al. 2000). To search

the databases⁴, J2000.0 coordinates as given in BAT99 were entered, and a search radius of $10''$ was applied in both cases. While MACHO yielded photometry of some of our targets (OGLE did not observe our programme stars), the data showed too large scatter to prove useful, most likely due to the brightness of our target stars. Thus, we did not carry out any further analysis of the photometry.

3 DATA REDUCTION

Some of our observation runs, notably those at the Cerro Tololo Inter-American Observatory (CTIO), were interrupted by other, time-critical observations, and thus split into several runs. Since the spectrograph had to be set up again each time, we treated each such run individually to allow for effects of different grating positions, angles, alignments, etc. Thus, a total of 13 individual runs were processed.

Data reduction was carried out in the usual way using the NOAO-IRAF software package⁵. Science data were corrected with average bias and flatfield frames, and object

² The *Chandra* Archive is available using the *Chandra* Search and Retrieval Interface (Chaser) at the *Chandra* X-ray Observatory site; see at <http://cxc.harvard.edu>.

³ The *ROSAT* Archive is supported by the High Energy Astrophysics Science Archive Research Center (HEASARC) of Goddard Space Flight Center, NASA. It can be accessed at the site <http://heasarc.gsfc.nasa.gov/W3Browse>.

⁴ Web interfaces for lightcurve retrieval from the respective databases are accessible at <http://www.macho.mcmaster.ca/> for MACHO, and at <http://bulge.princeton.edu/~ogle/> for OGLE

⁵ IRAF is distributed by the National Optical Astronomy Observatories, which are operated by the Association of Universities for Research in Astronomy, Inc., under cooperative agreement with the National Science Foundation.

spectra were optimally extracted using APALL with the 2D trace-fit option enabled. Sky background was fitted and subtracted from the stellar spectrum for all stars with the exception of those in the periphery of R136. This cumbersome task (cf. Selman & Melnick 2005) was deemed unnecessary because despite its strength, the discrete emission spectrum of the 30 Dor nebula does not affect the strategic WNL emission line, HeII $\lambda 4686$. It does however affect the (intrinsic) Balmer lines of these WNL stars, which renders the determination of the hydrogen content in the star highly uncertain. This has consequences which will be examined later.

Arc frames taken before and after each science exposure were averaged and then extracted. Unfortunately, due to the lack of good comparison lines at the blue edge of our spectra, the dispersion solution is less reliable in the region bluewards of 4400 Å. This had severe consequences for the precision of the radial-velocities measured from the NIV $\lambda 4058$ emission line, which yielded very large scatter. Extracted spectra were then rebinned to uniform stepwidth, corrected for heliocentric velocities, and rectified.

The spectra were then cleaned of cosmic rays and bad pixels as far as possible; where applicable, spectra from split exposures were combined. If a cosmic ray or bad pixel fell onto a strategic emission line, great care was taken not to significantly alter the original line profile. If this was not possible, the spectrum was discarded. The final stellar spectra were then rebinned to a uniform step-width of 1.65 Å/pixel, thereby yielding a conservative 3-pixel resolving power of $R \sim 1000$. The achieved S/N ratio per rebinned pixel, calculated for the spectral region from 5050 to 5350 Å, is 85 on average.

4 DATA ANALYSIS AND RESULTS

4.1 Radial-Velocity Measurements

Since in principle, we are mainly interested in *changes* in radial velocities (RVs) to identify the binaries, cross-correlation, which measures shifts relative to a template, was used as our main tool, since it yielded the smallest RV scatter.

In most of our WNL stars, the spectrum is dominated by the HeII $\lambda 4686$ emission, which is the strongest line by a wide margin. Thus, we concentrated our RV measurements on this emission line, restricting the cross correlation to the spectral region from 4600 to 4800 Å, which almost exclusively contains HeII $\lambda 4686$. To guard against an unlucky choice of template, we used an iterative approach for cross-correlation: For a first cross-correlation pass, a real, high-S/N spectrum from the data set of a given star was chosen as template. This template was cross-correlated with all other spectra. RV shifts were measured by fitting a Gaussian plus a (linear, rarely parabolic) continuum function to the cross-correlation profile. Resulting RVs were then used to shift all spectra into the template’s frame of reference. Then, a S/N-weighted average spectrum was computed using all shifted spectra, and used as a new template for a second cross correlation pass. Again, all spectra were shifted and added, and with this “supertemplate”, a final cross-correlation pass was made.

The advantage of this approach is that the resulting

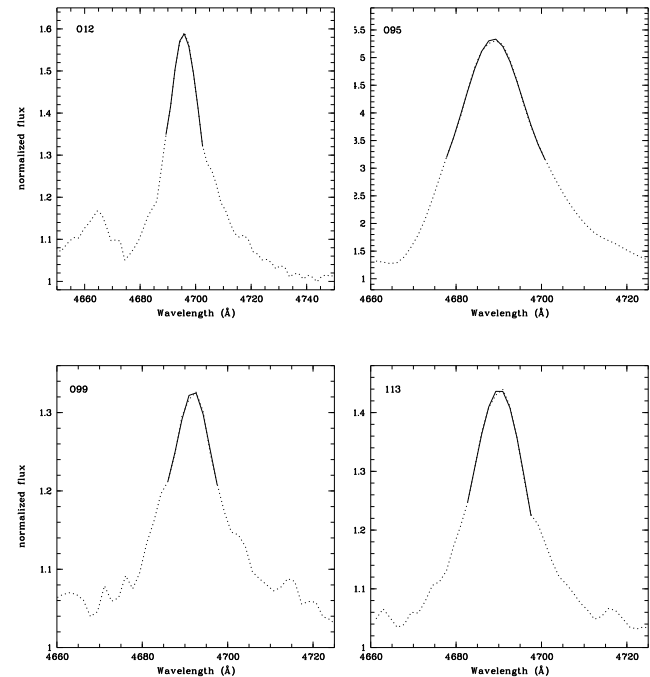


Figure 1. Examples of the HeII $\lambda 4686$ emission line (dotted) and Gaussian fits (solid) which were restricted to the upper part of the line. Shown are individual spectra with average S/N ratio of the four binaries which have been newly discovered in this study, BAT99-12, 95, 99 and 113.

supertemplate has a higher S/N than a single spectrum, and that (stochastic or cyclical) line-profile variations are mostly averaged out. The same is true for the potentially present spectral signature of a companion, which is maximally smeared out, because it moves in anti-phase to the WNL star⁶. While there were noticeable differences in RVs between the first and the second cross-correlation iteration, in most cases the third cross-correlation pass did not improve the RVs; still, it was carried out in all cases for the sake of uniformity.

Absolute (systemic) RVs were measured by fitting the HeII $\lambda 4686$ emission, whose peak was reasonably well reproduced by a single Gauss function (see Figure 1). Other lines were too weak and too noisy to be used, which is particularly unfortunate for the narrow, clean and rather symmetric NIV $\lambda 4058$ emission at the very blue edge of our spectra. This line also suffered from the lack of useful comparison-arc lines, which rendered impossible a reliable wavelength calibration (see Section 3), yielding a RV scatter more than twice as large as what was obtained from the HeII $\lambda 4686$ line.

While differences between RVs obtained from fits and from cross correlation remained remarkably small, direct fitting yielded a slightly larger RV scatter than cross correla-

⁶ This is particularly the case if the WN star is the more massive component of the binary system, as is possible in luminous WNL systems. The O star then shows the larger RV amplitude; its absorption lines are hence smeared out over a larger spectral region.

tion, most likely because of noise (in particular in weak-lined stars) and the line being slightly asymmetric. Potential intrinsic line-profile variability (e.g. due to wind-wind collision) might also add to the difference. Thus, whenever it was possible, we relied on RVs obtained by cross correlation rather than on those obtained by line-fitting.

4.2 Standard Stars and Systematic Shifts Between Observatories

Most stars show a small to very small RV scatter around or below 20 km s^{-1} (obtained by cross correlation). However, before identifying the binary stars in our sample, another potential problem had first to be taken care of. Foellmi et al. (2003a,b) reported systematic shifts between CASLEO and SAAO. Both observatories together with others were also used for our study; therefore, we had to make sure that any RV variation is of stellar origin and not a consequence of different (and possibly variable) instrumental zero points. In order to compute systematic shifts among the respective runs, we proceeded as follows: Of our 41 program stars, we selected those *i*) which are well isolated (no composite spectrum due to crowding), *ii*) for which RVs could be measured using cross correlation, *iii*) which displayed very small RV scatter, and *iv*) for which a preliminary period search in the period range from $1 \text{ d} \leq P \leq 200 \text{ d}$ did not yield cyclical RV variability (the period-search method is described more comprehensively below). Stars meeting these criteria are most likely true single stars or binaries with sufficiently long periods, large eccentricities, and/or low inclination angles that they can serve effectively, within our detection limits, as constant-RV standard stars. By construction, the only shifts these stars display are then solely due to systematic shifts among different observatories.

Twenty-three reference stars were thus selected (see Table 4). For each star, mean RVs were computed for each individual run. As described above, during the 2003/2004 campaign at CTIO (i.e. runs 11 through 13), a $1''$ slit width was used, hence the RV scatter is very small in these data sets, reaching a minimum during run 11 (see below). SSO displays a similarly small scatter, but there are many fewer points available. Thus, for better statistics, run 11 was chosen to provide the overall zero point. For each reference star, the mean RV of run 11, \overline{RV}_{11} , was subtracted from all RVs in order to normalize RVs to run 11. This was necessary because the cross-correlation method only yields relative RVs with respect to an arbitrarily chosen template, i.e. one that does not necessarily come from run 11. (Note that the shift-and-add method described above also suffers from this effect, because it starts out with one arbitrarily chosen spectrum.) Thus, for every individual star, $\overline{RV}_{11} = 0$, whereas for all other runs $j \neq 11$ in general $\overline{RV}_j \neq 0$. By construction, the respective values of these \overline{RV}_j are purely due, and directly correspond, to the systematic shifts among run 11 and all other runs.

However, not every star will display exactly the same shifts, but the shifts will be randomly distributed due to noise. By combining the 23 reference stars into one “super-reference”, we obtained the respective average mean velocities \overline{RV}_j per run – and thus directly the systematic shifts among run 11 and all other runs – as well as the standard deviations σ_j , which were adopted as empirical *a posteriori*

Table 4. List of the 23 fiducial RV standard stars together with their unweighted RV scatter.

BAT99	σ_{RV} kms^{-1}	BAT99	σ_{RV} kms^{-1}	BAT99	σ_{RV} kms^{-1}
13	12.5	55	14.6	93	20.5
16	13.3	58	14.7	96	18.7
22	13.3	76	15.5	97	19.6
30	17.3	79	14.3	100	15.4
33	16.2	80	20.5	120	21.8
44	15.8	83	14.9	130	13.2
45	11.4	89	14.3	133	15.4
54	18.2	91	13.7

Table 5. Systematic shifts between different runs and standard deviations of RV per run, used as *a posteriori* error bars. See text for details.

Run <i>j</i>	Observatory	RV shift kms^{-1}	σ_j kms^{-1}
1	CASLEO	-2.9	15.3
2	MSO	-16.1	19.0
3	CTIO	-3.0	20.9
4	CTIO	-10.7	13.3
5	SAAO	-8.7	17.2
6	CTIO	0.2	20.7
7	CTIO	-1.9	17.4
8	MSO	3.0	20.2
9	SSO	-24.9	10.4
10	LCO	-4.3	23.8
11	CTIO	0.0	10.3
12	CTIO	3.6	12.5
13	CTIO	-0.9	12.5

measurement errors for the RVs of the respective run *j*. Values range from 23.8 km s^{-1} at LCO (run 10) to 10.3 km s^{-1} at CTIO (run 11). Points from a given run *j* deviating from \overline{RV}_j by more than $\pm 3\sigma_j$ were rejected. (This σ -clipping on a per-run basis could not be done per individual star because there are not enough data points per run for meaningful statistics.) Both \overline{RV}_j and σ_j were then re-calculated; final values are given in Table 5. Systematic shifts could now easily be removed in *all* program stars by simply subtracting the respective values from all RVs of a given star and run.

RVs obtained by cross-correlation and corrected for systematic shifts are shown, for each season separately, in Figure 2. The dashed line indicates the zero mean velocity to which all RVs were normalized.

4.3 Random Variability and Significance Levels

Since we are looking for binaries, the property we are initially most interested in is *variability*, i.e. the standard deviation around the mean RV. After all, we expect binaries to show larger RV scatter than constant stars. But how large a scatter is large enough for a given star to be identified as variable? To distinguish stars which are most likely variable from those which, within the measurement errors, are not, we performed a χ^2 test. The idea is that if *all* stars in our sample were truly constant, RV measurements would be scattered around a mean velocity only due to random mea-

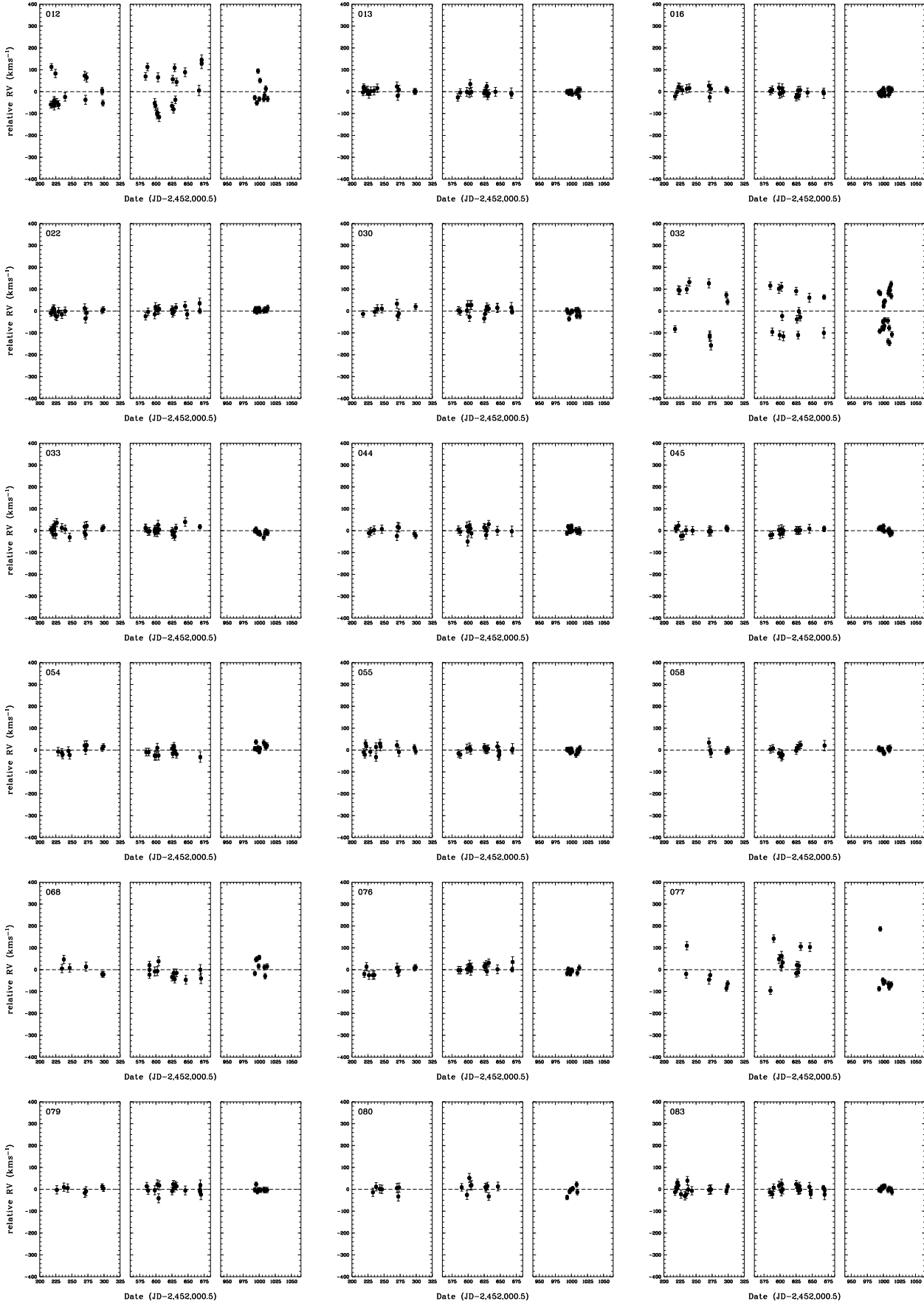


Figure 2. Relative RVs of our program stars for the three observing seasons.

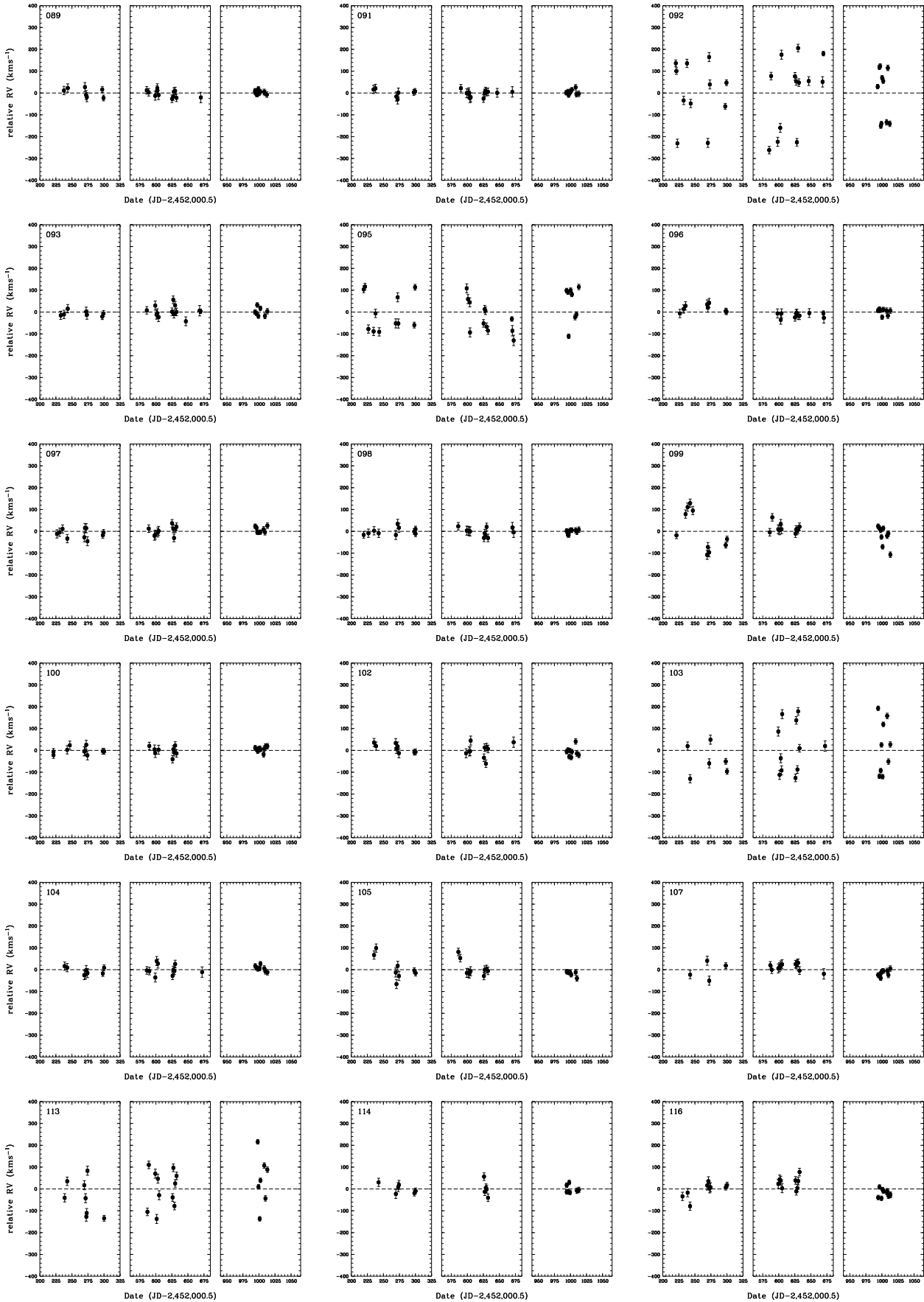


Figure 2 – *continued*

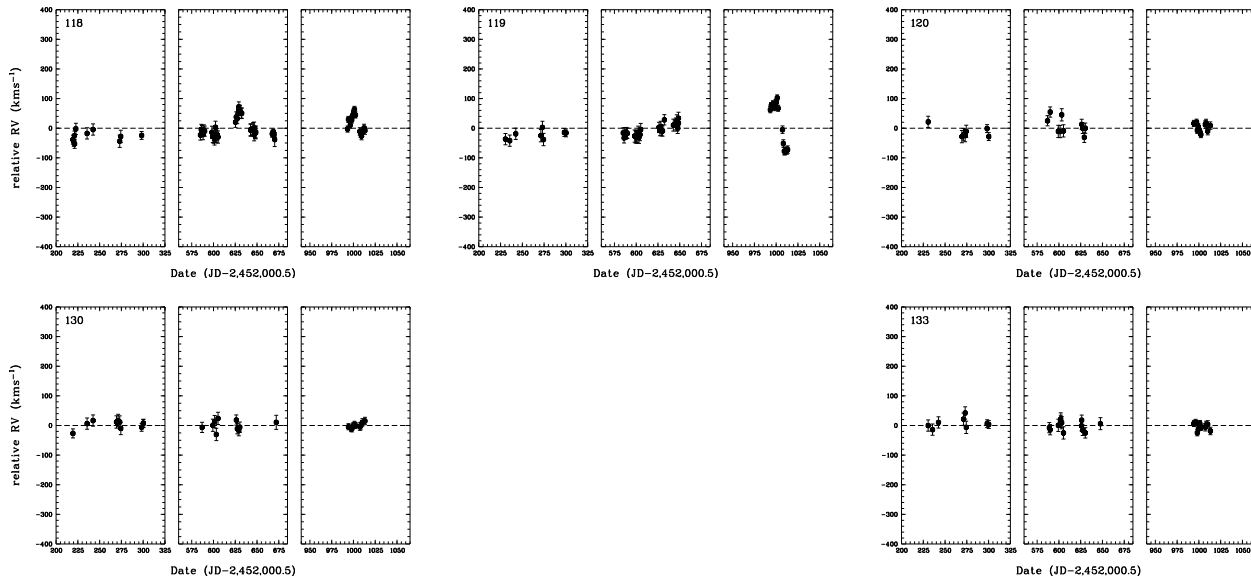


Figure 2 – continued

surement errors. In Figure 3, the 770 RV measurements of the 23 combined reference stars (the “super reference”) are shown in histogram form. A Kolmogorov-Smirnov test yields that this distribution is normal at a 99% confidence level, with $\overline{RV} = 0 \text{ kms}^{-1}$ and $\sigma = 16 \text{ kms}^{-1}$, a nice *a posteriori* confirmation to use those 23 stars as constant stars.

We now define the RV amplitude S be the span of RV such that 99.9% of the measured RVs fall within this span, i.e. $S = 3\sigma_{RV}$. For constant stars, the distribution of the *squared* RV amplitudes S^2 then follows a χ^2 distribution with df degrees of freedom, where df is the number of RV measurements per star (in our case, $df = 33$, because we have 33 data points per star on average). If a star displays a value of S^2 exceeding the 99.9% threshold, its RV scatter is not consistent with the hypothesis that it is a constant star; hence it will be considered variable.

A $\chi^2(x)$ function with $df = 33$ was computed. Values of the normalized x for $df = 30$ and a 99.9% level were taken from statistical textbooks (e.g. Kreyszig 1975) and linearly interpolated to $N = 33$ (which is usually not tabulated); we obtained $x = 64.1$. This corresponds to the cut-off value $S^2 = 5380 \text{ km}^2\text{s}^{-2}$ and thus $\sigma_{\text{cut}} = 22.6 \text{ kms}^{-1}$. Stars exceeding this threshold are considered variable at a 99.9% level (0.1% error probability); they are listed in Table 6. The observed RV square-amplitudes S^2 are shown in histogram form in Figure 4, with the χ^2 function overplotted after having been adjusted for the chosen bin-size. As we shall see further below, most, however not all, of the stars exceeding the 99.9 percentile also display periodicities in their RV curves, and indeed are binaries.

4.4 Cyclical Variability and Period Analysis

Variability, i.e. significantly large scatter, of RVs is not a sufficient criterion for *cyclical* variability, let alone for binarity. There are stars which are erratically variable, i.e. any measured RV scatter could be of stochastic nature. It is thus

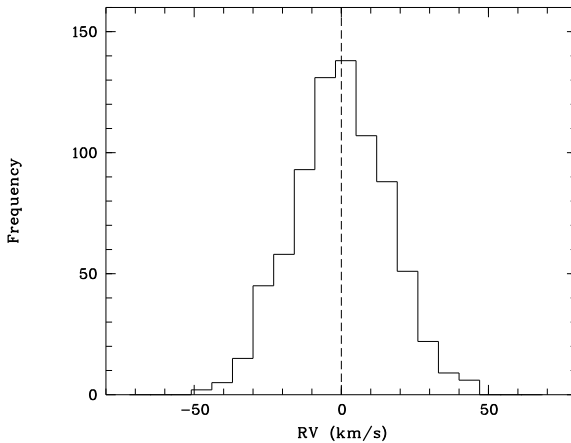


Figure 3. Histogram of RV measurements of the 23 reference stars, obtained by cross-correlation, and after correction for systematic shifts. In total, 770 data points are used. Binsize is 7 kms^{-1} . The unweighted standard deviation around the mean is 16 kms^{-1} .

Table 6. Stars whose RV standard deviation σ_{RV} exceed the cut-off value of 22.6 kms^{-1} and which therefore are considered variable.

BAT99	σ_{RV} [kms ⁻¹]	BAT99	σ_{RV} [kms ⁻¹]
12	70.8	103	106.7
32	92.4	105	37.7
68	29.5	107	23.9
77	78.2	113	93.3
92	139.8	116	32.6
95	81.6	114	23.2
99	58.9	118	31.6
102	25.3	119	44.7

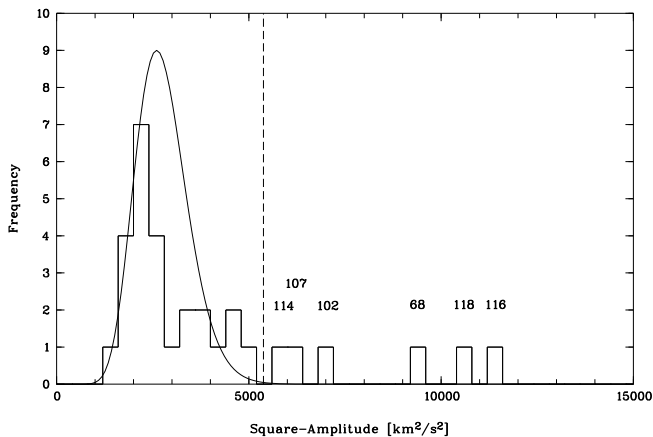


Figure 4. Histogram of square-amplitudes S^2 of our program stars with the χ^2 distribution for $\sigma = 16 \text{ km s}^{-1}$ overplotted. Bin-size is $400 \text{ km}^2 \text{ s}^{-2}$. The dashed vertical line indicates the cut-off value corresponding to $\sigma_{\text{RV}} = 22.6 \text{ km s}^{-1}$; stars to the right of this cut-off are considered variable at a 99.9% confidence level. They are named by their respective BAT99 number. Note that ten stars in our sample have square-amplitudes larger than $15,000 \text{ km}^2 \text{ s}^{-2}$ (corresponding to RV scatters $\sigma_{\text{RV}} > 37.8 \text{ km s}^{-1}$). For reasons of clarity, they are not shown in this diagram, but listed in Table 6.

important to verify whether or not any star shows periodic RV variabilities.

4.4.1 Period-Search Algorithms

After having corrected all data sets for systematic shifts, we re-performed a period search on the unweighted RVs of *all* stars in the period range from 1 to 200 days, using a code by Kaufer et al. (1996). In each step of the iteration, this code computes CLEANed periodograms and window functions of unevenly distributed data points according to Deeming (1975; see also Schwarz 1978; Roberts et al. 1987). Significance levels are calculated for the found periods using Lomb-Scargle statistics (Lomb 1976; Scargle 1982), i.e. by fitting sine waves to the data points and minimizing the χ^2 . Of those peaks that exceed the 3σ significance level, the one with the highest power is selected, and its half width at half maximum is adopted as $1-\sigma$ error on the period.

Our observations are fragmented into 13 runs of different duration and slightly different typical sampling frequencies between 0.5 and 2 data points per day and per star. This somewhat reduces aliasing problems, although $1 - \nu$ aliases remain well visible in most periodograms. For non-circular orbits, where significant power can be contained in the harmonics of the fundamental frequency, even more side-band peaks are generated, since the harmonics themselves suffer from aliasing. However, neither fitting higher-order terms of the Fourier expansions (up to third order) nor using the analysis-of-variance (AOV) algorithm (cf. Schwarzenberg-Czerny 1989) changed the results significantly. Thus, only results obtained with Lomb-Scargle statistics are quoted.

4.4.2 Stars With Periodicities

Periodograms of identified cyclically variable stars are shown in Figure 5. Almost all binary periods reported by previous studies (Moffat 1989, and references therein) were reproduced with remarkable similarity, and by combining our data with published data, we were able to further increase the accuracy of the periods (see Table 7). These revised periods were used in the further analysis. The confirmed binaries are BAT99-32, 77, and 92.

BAT99-77 is an eccentric binary system with an almost perfect 3-day period which is why it displays a forest of significant frequency peaks, harmonics, and aliases. This makes it difficult to determine which period is the correct one; however, only the 3-day period yields a coherent RV curve, and a full Keplerian fit to BAT99-77’s RVs confirms the result (see Section 4.5).

In one curious case, the 2.76-day period reported for BAT99-102 (R140a2) was clearly found, however in its *neighboring star*, BAT99-103 (R140b). Careful inspection of our logbooks did not reveal any possible confusion at the telescope, nor is there any indication of such a mishap in Moffat et al. (1987), who first detected the binary. BAT99-102 forms a visual pair with BAT99-101 (R140a1) which even under the best seeing conditions at CTIO could not be separated. Both stars lie very close to BAT99-103, and given our relatively large slit width, some cross-contamination of emission lines is not impossible, which could lead to a detection of the same periodicity in BAT99-102, too. While we cannot propose a solution to this issue, we will from here on consider BAT99-103 as the 2.76-day binary.

Four new stars were found to display periodic RV curves: BAT99-12, 95, 99, and 113. None of these four stars was included in the study of Moffat (1989), either because it was not listed as a WR star in previous Catalogue versions, or because it was too faint for Moffat’s magnitude-limited sample ($V \leq 13$ mag). Note, however, that BAT99-99 is at the detection limit, as is clearly illustrated by the periodogram in which the highest peak is not very clearly pronounced; also, a full Keplerian fit did not converge (see Section 4.5), so that the 92.6-day period has to be considered very preliminary.

4.4.3 Stars Without Periodicities

For most stars with a small RV scatter below the variability threshold, in particular the 23 reference stars, no periods at all were found, i.e. not even spurious ones. This is also the case for BAT99-107, for which Moffat (1989) had reported a 52.7-day period and for which no period whatsoever was detected. For some few stars, marginally significant frequencies were identified, but the data points yielded incoherent RV curves when folded into the corresponding phases. Hence, we have discarded these periods as spurious.

For BAT99-119, we did not reproduce the tentative 25.4-day (assumed circular-orbit) period reported by Moffat (1989), but it was identified as significantly variable (see Section 4.3). Indeed, by combining our RV data with that of Moffat, we were able to establish the binary nature of BAT99-119, although it was only after combining the RV data with unpublished polarimetry that the correct period

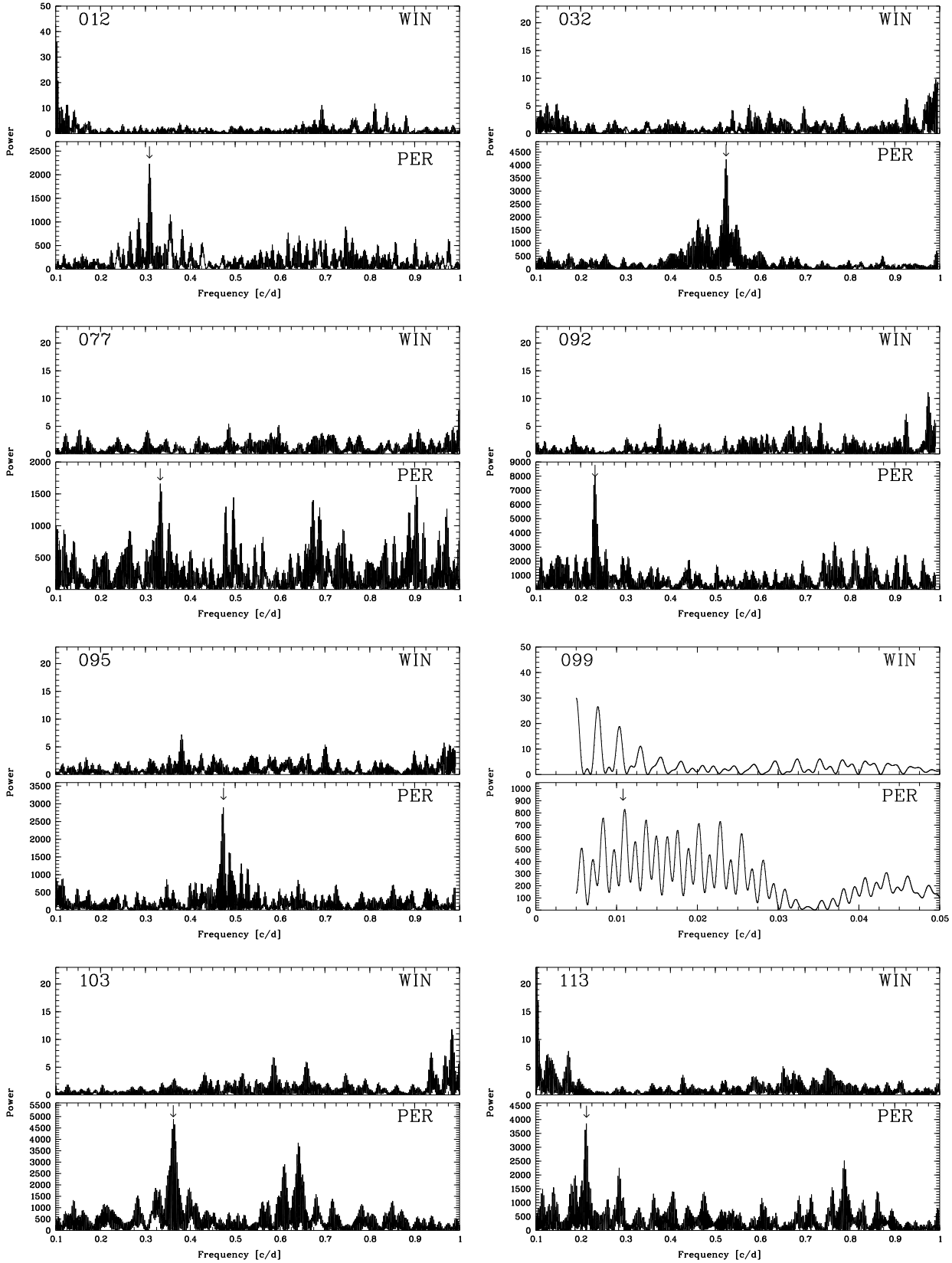


Figure 5. Window functions (WIN, *upper panels*) and periodograms (PER, *lower panels*) in the period range of 1 to 100 days (for BAT99-99: 20 to 200 days), expressed in cycles per day (c/d). BAT numbers are indicated. The frequency peak corresponding to the period quoted in this study is indicated by an arrow. Note the strong differences in *y*-scale between the window functions and the periodograms.

Table 7. Periods (in days) found for our program stars in this work and previous studies. Newly identified, periodically variable stars are indicated. References are: (1) Moffat & Seggewiss (1986); (2) Moffat (1989); (3) Moffat et al. (1987; but see text for details).

BAT99	previous studies	this work	combined data	Ref.
12	n/a	3.2358 ± 0.0058	n/a	new
32	1.9075 ± 0.0002	1.9075 ± 0.0015	1.90756 ± 0.00012	1
77	3.0032 ± 0.0002	3.0034 ± 0.0042	3.00303 ± 0.00029	2
92	4.3092 ± 0.0040	4.311 ± 0.008	4.3125 ± 0.0006	2
95	n/a	2.1110 ± 0.0018	n/a	new
99	n/a	92.60 ± 0.31	n/a	new
103	2.7596 ± 0.0001	2.7597 ± 0.0038	2.75975 ± 0.00027	3
113	n/a	4.699 ± 0.010	n/a	new

of $P = 158.8$ days and an orbital solution could be found (Schnurr et al., in prep.). Since the system has a long-period *and* a highly eccentric ($e \sim 0.7$) orbit, we are clearly limited by the phase coverage of our data; had it not been for the polarimetry, we would have missed the binarity of BAT99-119. On the other hand, we can reasonably assume that we are just able to detect (circular) binaries with orbital period up to ~ 100 days, given that we were able to identify BAT99-99 as a binary as establish a tentative period of ~ 92 days. A detailed discussion of our detection limits is given in Section 5.1).

4.5 Binaries: The Remaining Orbital Parameters

For variable stars with identified, coherent periods, we attempted to compute orbital parameters using the program ELEMENTS (cf. Marchenko et al. 1994). This code allows one to assign weights $1/\sigma_{\text{RV}}^2$ to each data point, according to its *a posteriori* measurement errors determined in Section 4.2 on a per-run basis (Table 5). As input guess for the orbital period, we used the value which was obtained from the CLEAN analysis of the *unweighted* data points, and when available, we used the periods obtained from the combined data sets (see above). Since we however did apply weights for the fit of the orbital solution, we did not fix the period but kept it as a free fitting parameter. In all cases, the periods found by ELEMENTS were, within the errors, identical to those obtained from our CLEAN analysis of either our or the combined data set. Fixing the value did thus not significantly change the orbital solution nor the errors. However, we again applied an iterative approach. For each data point j , ELEMENTS returns the value *observed minus computed*, $(o - c)_j$. After the first pass of ELEMENTS, we computed the overall mean $\overline{o - c}$ and the standard deviation from this mean, i.e. σ_{o-c} . Any data point j with $|(o - c)_j| > 3\sigma_{o-c}$ was removed from the data set, and the orbital solution was fitted again. This procedure was repeated until all data points were within $3\sigma_{o-c}$ of the fitted orbital solution. Usually, this happened after the third iteration, which means that only few data points had to be discarded. Naturally, the final orbital period no longer agreed with the initial guess, because the underlying data set had been modified. Yet, deviations remained very small.

In all cases where the algorithm converged, ELEMENTS returned an elliptical orbital solution, although e was small in most cases. Therefore, we repeated the fit and forced a circular solution by imposing $e = 0$, with $\phi = 0$ defined at

the time E_0 of inferior conjunction, when the WR passes in front of its companion; thus, E_0 is different from the time of periastron passage, T_0 , returned from the elliptical fit. Both sets of parameters are given in Table 8; parameters that were fixed for the circular fit are indicated by the symbol “@” after the value.

In all cases but for BAT99-77, the overall quality of the fit, expressed by σ_{o-c} , did not significantly deteriorate. Thus, for the rest of this study the circular solution was adopted for all stars, with the exception of BAT99-77. To illustrate the differences between the free, elliptical solution and the forced, circular one, both solutions are shown in Figure 6. Plotted are all data points which have been retained for the fit after having applied the iterative σ clipping described above. For the purpose of graphical comparison only, the circular solutions shown were computed using $E_0 = T_0$ of the given elliptical case, so that their zero phases coincide for better clarity. Note that in the tables, the dates for E_0 and T_0 are different.

In the following, we will discuss the binary status of individual stars which display cyclical RV variability.

— **BAT99-12:** This newly identified variable shows a clear periodicity of 3.2358 days in its RV curve obtained from the HeII $\lambda 4686$ emission lines. Although the RV curve is somewhat noisy when the RV points are folded into the corresponding phase, the orbital fit converges. The obtained eccentricity is surprisingly large for such a short-period orbit. This might be because the HeII $\lambda 4686$ emission is subject to severe distortions due to WWC. Forcing a circular fit deteriorates the overall error σ_{o-c} only slightly, so that a circular motion with slightly changed orbital parameters was adopted for the rest of the paper. The systemic velocity γ obtained from the orbital fit is very large, $\gamma = 650 \pm 8 \text{ km s}^{-1}$, and qualifies this system for a fast runaway binary (see also Massey et al. 2005). This is very remarkable given the fact that such close and massive binary systems are very “hard” with respect to gravitational interactions with other cluster members. This object clearly deserves more attention; we have therefore obtained higher-quality, follow-up observations which will be the subject of a future study.

— **BAT99-32:** This star is a known binary with an orbital period of 1.9076 days, the shortest known among the WN binaries in the LMC; yet it does not display the largest RV amplitude (see BAT99-92). This might indicate that the system is seen under a low inclination angle. Within the errors, the system has a circular orbit, as might be expected for such short systems.

— **BAT99-77:** This star is a known binary with an al-

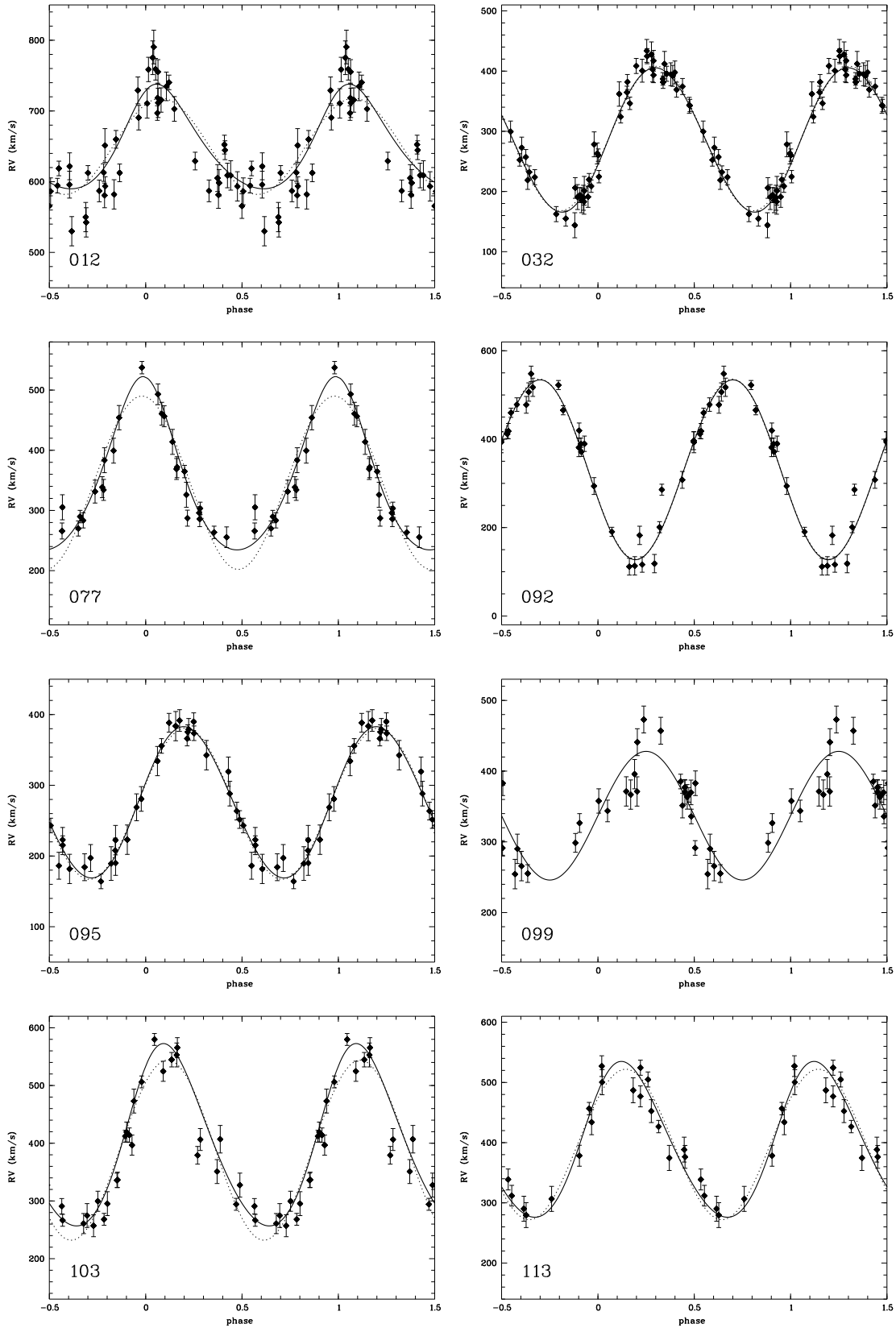


Figure 6. Orbital solutions for the binary systems, folded into the respective phases. Shown are both the solution for the elliptical (solid) and the circular (dotted) orbit.

Table 8. Orbital parameters for the WR component of our binary systems. Results are given for both the free, elliptical fit and the forced, circular solution. For the latter, ω is not defined (n/d). Depending on the eccentricity of the orbit, zero-phase ϕ_0 is either the time of periastron passage, T_0 , or the time of inferior conjunction (i.e., WR star in front), E_0 .

BAT99	P (days)	e	K (kms $^{-1}$)	ω ($^{\circ}$)	γ (kms $^{-1}$)	ϕ_0 (HJD-2,400,000.5)	σ_{o-c} [km/s]
12	3.2358 ± 0.0058	0.34 ± 0.06 0	74 ± 5 68 ± 8	-29 ± 11 n/d	642 ± 13 650 ± 8	52269.84 ± 0.09 52272.58 ± 0.10	24.8 27.1
32	1.90756 ± 0.00012	0.06 ± 0.02 0	120 ± 3 120 ± 3	250 ± 22 n/d	288 ± 6 288 ± 6	53011.57 ± 0.12 53011.68 ± 0.12	13.5 14.2
77	3.00303 ± 0.00029	0.32 ± 0.02 0	144 ± 4 144 ± 15	7 ± 4 n/d	333 ± 8 346 ± 10	52631.87 ± 0.04 52637.05 ± 0.06	10.9 16.9
92	4.3125 ± 0.0006	0.02 ± 0.02 0	204 ± 5 204 ± 5	109 ± 66 n/d	332 ± 7 332 ± 7	52998.03 ± 0.04 52999.96 ± 0.04	16.8 17.0
95	2.1110 ± 0.0018	0.07 ± 0.03 0	107 ± 3 107 ± 3	285 ± 18 n/d	274 ± 9 274 ± 9	52999.87 ± 0.10 52999.78 ± 0.09	10.6 10.9
99	92.60 ± 0.31	0	91 ± 19	n/d	337 ± 16	53045.90 ± 1.30	30.5
103	2.75975 ± 0.00027	0.23 ± 0.03 0	158 ± 4 156 ± 10	-41 ± 7 n/d	388 ± 8 388 ± 8	53007.80 ± 0.05 53010.22 ± 0.05	19.9 23.8
113	4.699 ± 0.010	0.20 ± 0.05 0	130 ± 8 125 ± 15	308 ± 16 n/d	390 ± 10 397 ± 11	52993.07 ± 0.13 52992.53 ± 0.14	18.1 20.5

most integer-day period which makes it hard to determine. However, the orbital fit confirms our period, and yields quite a large eccentricity for such a short system. Consequently, the overall error increases significantly when a circular solution is imposed. Presently, we do not have enough data to confirm whether this is due to WWC-induced distortions of the HeII $\lambda 4686$ emission or whether the orbit is indeed non-circular, but for the rest of this paper, we adopt the elliptical solution.

— **BAT99-92:** This star is a known binary. The orbital fit yields a remarkably small eccentricity, so that the circular solution is adopted. This system shows the largest RV amplitude of our program stars, although it does not have the shortest period. This might indicate that it is seen under a large inclination angle, which renders BAT99-92 potentially interesting for a photometric campaign to obtain the inclination angle from a light curve.

— **BAT99-95:** This is a newly discovered binary in the 30 Dor region. Despite its short orbital period, it has a remarkably small RV amplitude. A circular solution is adopted for this system.

— **BAT99-99:** This is a newly discovered binary system located in the periphery of the R136 cluster in the center of the 30 Dor region. Massey et al. (2005) has reported this star to be a binary, but not given an orbital period. From our analysis, we find a rather long period of 92.6 days, close to our detection limits (see above). Unfortunately, folding the data points into the corresponding phase yields a rather noisy RV curve. A free (elliptic) fit does not converge, so that we have forced a circular solution; however, σ_{o-c} is uncomfortably large, probably because the true orbit is elliptical indeed. We thus report a tentative set of orbital parameters for BAT99-99. Errors on individual parameters are not stated, rather we quote the σ_{o-c} of the total solution.

— **BAT99-103:** This star is a known binary system, located in the periphery of the R136 cluster. Again, we are unable to verify whether or not the non-zero, albeit mild eccentricity is real, but the circular fit is only moderately worse.

Since the RV curve is not very clean, both WWC-induced distortions and the weakness of the HeII $\lambda 4686$ emission line are the most likely causes for this result.

— **BAT99-113:** This is a newly discovered binary system in the periphery of R136. Regarding the non-zero eccentricity, the same remarks apply as for the previous system.

4.6 Systemic Velocities and Runaway Stars

For single program star, both mean $\overline{RV}_{\text{sys}}$ and standard deviations were computed from RVs obtained through Gauss fits to the HeII $\lambda 4686$ emission line (see Section 4.1). For binary stars, the systemic velocity γ and its error returned from the orbital fit were used. Resulting $\overline{RV}_{\text{sys}}$ are listed in Table 9 and shown in histogram form in Figure 7.

Averaged over our complete sample, we find 314 ± 10 kms $^{-1}$, somewhat more than the systemic velocity of the LMC, which is 280 ± 20 kms $^{-1}$ (e.g. Kim et al. 1998), but consistent with the value Foellmi et al. (2003b) reported for their WNE sample stars, 324 ± 6 kms $^{-1}$. However, we re-analyzed Foellmi et al.’s data and found 345 ± 6 kms $^{-1}$, which is then incompatible with our results for WNL stars. The origin of this systematic difference is not entirely clear, but most likely stems from the way the measurement were carried out; we used line-fitting, while Foellmi et al. used bisectors on selected parts of the HeII $\lambda 4686$ emission line. For consistency, we will use our values in the following discussion. In Table 10, the systemic velocities of the different subsamples are shown; all errors quoted are the error of the mean ($com = \sigma_{\text{RV}}/\sqrt{N}$).

The measured redshift does not come unexpectedly; it is well known among observers that some emission lines of WR stars yield redshifted systemic velocities. Some authors have attributed this phenomenon to a prominent electron-scattering wing on the red flank of the emission line (e.g. Auer & van Blerkom 1972), others to the presence of a blue-shifted P Cygni absorption, diminishing the blue flank of the emission profile (e.g. Bartzakos et al. 2001). Hillier

Table 9. Systemic velocities and RV scatter for our program stars.

BAT99	$\overline{RV}_{\text{sys}}$ [kms $^{-1}$]	σ_{RV} [kms $^{-1}$]	Binary?	remarks
12	650	70.8	yes	runaway
13	277	12.5
16	330	13.3
22	255	13.3
30	345	17.3
32	288	92.4	yes	...
33	293	16.2
44	398	15.8
45	245	11.4
54	316	18.2
55	140	14.6	...	runaway?
58	311	14.7
68	321	29.5
76	274	15.5
77	333	78.2	yes	...
79	288	14.3
80	374	20.5
83	...	14.9
89	303	14.3
91	324	13.7
92	332	139.8	yes	...
93	373	20.5
95	274	81.6	yes	...
96	274	18.7
97	305	19.6
98	321	14.7
99	337	58.9	yes	...
100	307	15.4
102	317	25.3	?	...
103	388	106.7	yes	...
104	342	18.4
105	273	37.7
107	303	23.9
113	397	93.3	yes	...
114	393	23.2
116	373	32.6
118	301	31.6	?	...
119	332	44.7	yes	...
120	282	21.8
130	287	13.2
133	280	15.4

(1989), on the other hand, explains the observed redshift by radiative-transfer effects in optically thick lines⁷.

Both Foellmi et al. (2003b, their Figure 8) and Bartzakos et al. (2001, their Figure 8) reported a negative correlation between the line width (FWHM) and the measured systemic velocities, showing that broader lines better reflected the true systemic (i.e. LMC) velocity. However, after combining the data sets for the WNL and WNE stars, we found that to the contrary, there is a *positive* correlation between the linewidth and the measured systemic velocities; the combined data are shown in Figure 8. Furthermore, we have binned stars to certain FWHM ranges, and calculated the bin mean systemic velocity and its error. The results are listed in Table 11. Indeed it seems that *only* the most

⁷ We are indebted to the anonymous referee for pointing this out to us.

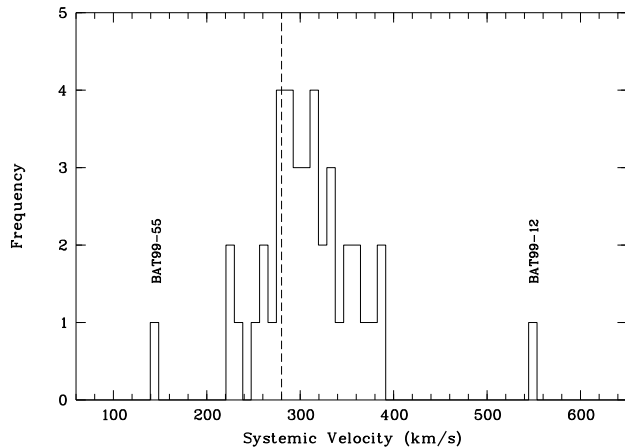


Figure 7. Histogram of mean systemic velocities of our program stars as measured by Gauss fits to the HeII $\lambda 4686$ emission line. The dashed vertical line indicates the expected systemic velocity of the LMC, 280 kms $^{-1}$. Note the two outliers, BAT99-12 and BAT99-55; these are most likely runaway stars. See text for more details.

narrow-lined WNL stars (FWHM $\lesssim 500$ kms $^{-1}$) do correctly reflect the systemic velocity of the LMC, whereas broader-lined stars, i.e. those with optically thicker winds, *on average* yield redder systemic velocities, in line with Hillier’s (1989) explanation. Note that contrary to what Foellmi et al. (2003b) reported, the measured systemic velocities for stars with FWHMs broader than 500 kms $^{-1}$ remain essentially constant at ~ 330 kms $^{-1}$, rather than to converge again towards the true LMC value.

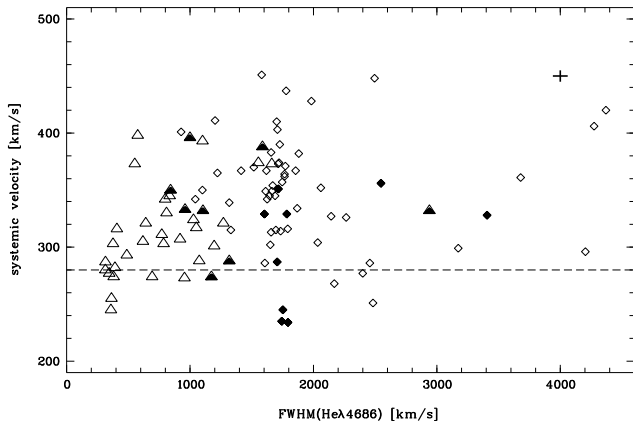
Two interesting cases, BAT99-55, a constant star, and BAT99-12, a binary, are marked in Figure 7 with their names. These stars have systemic velocities which are quite different from the systemic velocity of the LMC, 146 kms $^{-1}$ (BAT99-55) and 650 kms $^{-1}$ (BAT99-12; circular orbit assumed), respectively. Thus, these stars are excellent runaway candidates (for a definition of runaway stars, see Blaauw 1961). Moreover, Massey et al. (2005) report a systemic velocity of 430 kms $^{-1}$ for BAT99-12, obtained from absorption lines in their better-resolved spectra, confirming its high systemic velocity; our much larger velocity is most likely an artefact due to the mentioned P Cygni absorption in the blue flank of the HeII $\lambda 4686$ emission line. The runaway nature is another property that BAT99-12 shares with its Galactic counterpart, the O4Infl star ζ Pup.

4.7 Mean Spectra and Spectral Types

Spectra from individual observatories were concatenated to obtain an average, high-S/N spectrum. To verify the spectral types listed in the BAT99 catalogue, the classification criteria of Smith et al. (1996; hereafter SSM96) were applied. In most cases, the change in spectral type was only very minor; results are listed in Table 12. The most important change is BAT99-92, which is also a confirmed binary. This star is listed as WN6 (cf. Moffat & Seggewiss 1986), but closer inspection of the spectrum reveals that BAT99-92 is hotter. However, its true spectral type is very difficult

Table 11. Mean systemic velocities of stars binned into different FWHM ranges. N is the number of stars per FWHM bin, \overline{RV} the mean systemic velocity, σ the RV scatter, and $eom = \sigma/\sqrt{N}$ the error of the mean systemic velocity in the respective bin.

FWHM [kms^{-1}]	0-500	500-1000	1000-1500	1500-2000	2000+
N	10	16	16	40	17
\overline{RV} [kms^{-1}]	281	335	333	335	332
σ [kms^{-1}]	21	41	38	49	55
eom [kms^{-1}]	6.6	10.3	9.5	7.7	13.3

**Figure 8.** Mean systemic velocities plotted against the FWHM (in velocity units) of HeII $\lambda 4686$ emission line for the WN stars in the LMC. Triangles denote the 41 WNL stars, lozenges denote the 61 WNE stars. Filled symbols are identified binaries. The dashed line indicates the systemic velocity of the LMC ($\sim 280 \text{ kms}^{-1}$). For clarity, error crosses have been omitted, but a typical error cross ($\pm eom = \pm \sigma/\sqrt{N}$) is shown in the upper right-hand corner. Most stars have larger systemic velocities than the LMC, and the star-to-star scatter is significant. The two runaway candidates, BAT99-12 and 55, have been omitted for this graph so that the y axis is not unduly compressed. See text for more details.**Table 10.** Average systemic velocities for different WN samples in the LMC, as observed by this study (WNL, including the O3f/WN6 stars) and by Foellmi et al. (2003b; WNE). Values are in kms^{-1} .

Subsample	$\overline{RV}_{\text{sys}}$
WNL, all	314 ± 10
WNL, no binaries, no runways	305 ± 7
WNE, all	345 ± 6
WNE, no binaries, no runways	353 ± 6
WN, all	334 ± 5
WN, no binaries, no runways	338 ± 5
LMC	280 ± 20

to determine because of the dominating B supergiant spectrum. We tentatively assign a WN3:b(+O)+B1Ia type to this system.

We have also measured both the full-width at half maximum (FWHM) and the equivalent width (EW) of the HeII $\lambda 4686$ emission line (see Table 12), with their standard deviations of the time series σ_{EW} as errors. Both for crowded stars, whose dilution depends on seeing or slit-positioning,

and for weaker-lined stars such as O3If/WN6 stars, σ_{EW} can be rather large. FWHMs, however, remain unaffected by dilution effects, with measurement errors of the order of 10 to 15% in all cases. Of course, some stars might be intrinsically variable, but an in-depth study of the line-variability phenomenon and its underlying causes is a very complex task and beyond the scope of the present paper. Results of such a study are planned for a future paper.

Many of our program stars still contain residual hydrogen, and some are even expected to be still in the CHB phase. The main indicator for the presence of H in the WR spectrum is the alternating HeII Pickering decrement. If not stated otherwise, nebular lines did not hamper the spectral classification. In the 30 Dor region, however, the alternating Pickering decrement of helium lines suffers considerably from nebular pollution, and the determination of the H content remains (very) uncertain; such subtypes feature a “:” (or even “::”) to indicate this uncertainty. Note also that the unsubtracted nebular emission leads to partially filled-up absorptions. Together with our relatively low spectral resolution, which affects narrower absorption lines more than broader emission lines, some O3If/WN6 stars, whose very weak HeII $\lambda 4686$ emission lines (small EWs) clearly distinguishes them from genuine WN stars (Walborn 1986), display an artificially attenuated absorption-line spectrum, thus favoring a (diluted) WN- rather than an O-star classification. Indeed, Massey et al. (2004, 2005) proposed the O2If classification for some of the O3If/WN6 stars using higher-resolution data and applying the criteria of Walborn et al. (2002). Nevertheless, two hot slash-stars were reclassified into WN types, BAT99-80 (now WN5ha:) and BAT99-105 (now WN7), based on the relatively large EW and the presence of a HeII $\lambda 5411$ emission. Their spectrum resembles that of genuine, yet diluted WN stars. In turn, BAT99-68 is listed as WN5-6 in the BAT99 catalogue, although it was classified as Of by SSM96. This star is located in a cluster, hence its spectrum is severely diluted. However, because of both the weak EW and the absence of a HeII $\lambda 5411$ emission line, we re-classify this star as Of/WN7, the WN part of the spectral type being based on the emission-line spectrum.

Regarding the Ofpe/WN9 or “cool slash-stars”, we did not re-classify them, since most of them have already been re-classified into WN10-11 by Crowther & Smith (1997), and we maintain this classification. The exception is BAT99-33 (R99), which has already been reported to show a peculiar spectrum that is inconsistent with a WR classification (see Crowther & Smith 1997 for more details). We thus maintain the Ofpe/WN in our Table 12, but add a “?”. In the case of BAT99-107, which is listed as WNL/Of, we change the spectral type to WN9h::a.

A montage of the (re-)classified, mean spectra of each of our program stars are displayed in Figure 9. Note that for

Table 12. Spectral types, and equivalent width (EW) and full-width at half maximum (FWHM) of the HeII $\lambda 4686$ emission line of our program stars. Spectral types that have been changed by us are also given.

BAT 99	Spec. Type (BAT99)	Spec. Type (this work)	EW [Å]	FWHM [Å]
12	O3If*/WN6		-12.3 ± 1.6	17.9 ± 1.9
13	WN10		-2.7 ± 0.3	5.4 ± 0.7
16	WN8h	WN7h	-40.2 ± 1.3	12.7 ± 0.3
22	WN9h		-4.6 ± 0.5	5.7 ± 0.7
30	WN6h		-50.0 ± 1.5	13.1 ± 0.3
32	WN6(h)		-74.0 ± 3.8	20.6 ± 2.0
33	Ofpe/WN9	Ofpe/WN9?	-2.8 ± 0.7	7.6 ± 0.7
44	WN8h	WN8ha	-26.8 ± 1.0	9.0 ± 0.3
45	WN10h			
54	WN9h	WN8ha	-7.2 ± 0.8	6.4 ± 0.4
55	WN11h		-0.5 ± 0.2	4.7 ± 1.5
58	WN6h	WN7h	-38.8 ± 1.3	12.1 ± 0.2
68	WN5-6	Of/WN7	-6.1 ± 1.5	10.0 ± 1.0
76	WN9h	WN9ha	-8.4 ± 0.6	6.0 ± 0.5
77	WN7	WN7ha	-11.4 ± 3.1	15.0 ± 1.6
79	WN7+OB	WN7ha+OB	-26.0 ± 0.8	16.8 ± 0.8
80	O4If/WN6	WN5h:a	-9.2 ± 1.5	24.3 ± 3.3
83	Ofpe/WN9	LBV		
89	WN7h		-65.8 ± 2.1	12.3 ± 0.7
91	WN7	WN6h:a	-10.5 ± 3.0	16.1 ± 0.5
92	WN6+B1Ia	WN3:b(+O) +B1Ia	-13.5 ± 1.2	46.0 ± 3.6
93	O3If/WN6		-4.8 ± 0.5	8.6 ± 1.3
95	WN7h	WN7	-84.6 ± 9.8	18.4 ± 1.1
96	WN8(h)	WN8	-26.4 ± 6.0	10.8 ± 0.8
97	O3If*/WN7		-6.2 ± 1.6	9.7 ± 1.1
98	WN6(h)	WN6	-19.4 ± 6.2	19.9 ± 1.7
99	O3If*/WN6		-4.1 ± 0.6	13.2 ± 1.5
100	WN6h	WN7	-26.5 ± 3.6	14.4 ± 1.7
102	WN6+O	WN6	-21.5 ± 4.3	16.4 ± 2.0
103	WN6		-27.1 ± 5.7	24.8 ± 3.5
104	O3If*/WN6		-4.2 ± 0.6	12.5 ± 1.5
105	O3If*/WN6	WN7	-18.7 ± 5.2	14.9 ± 1.8
107	WNL/Of	WN9h::a	-1.7 ± 0.4	5.9 ± 0.7
113	O3If*/WN6		-5.1 ± 1.6	15.6 ± 1.2
114	O3If*/WN6		-3.5 ± 0.6	17.2 ± 1.5
116	WN5h	WN5h:a	-29.5 ± 6.5	26.0 ± 0.8
118	WN6h		-60.0 ± 2.9	18.7 ± 0.9
119	WN6h		-50.7 ± 4.1	17.3 ± 1.1
120	WN9h		-5.0 ± 1.5	6.1 ± 0.3
130	WN11h		-1.3 ± 0.2	4.9 ± 0.6
133	WN11h		-1.1 ± 0.2	4.9 ± 0.6

stars in the 30 Dor region, nebular lines have been clipped; thus, in some spectra, the H β and H γ lines are truncated.

4.8 Analysis of the X-Ray Data

Chandra and *ROSAT* archives were searched for X-ray emission from the WNL stars in the LMC. We first extracted *Chandra* ACIS X-ray images in the 0.3–7.0 keV energy band, and *ROSAT* PSPC and HRI images in the full energy range of these instruments, i.e., 0.1–2.4 keV for the PSPC and 0.1–2.0 keV for the HRI. We then compared these X-ray images with optical images extracted from the Digitized Sky

Survey⁸ (DSS). We identified each WR star in the optical images using the coordinates listed by BAT99, and then searched for X-ray emission at the location of the WR star.

X-ray emission is detected in 15 WNL stars in the LMC, as indicated in Table 13. To confirm these detections, we defined source regions encompassing the X-ray sources at the location of the WR stars and appropriate background regions. The background-subtracted count number and count rates are also listed in Table 13. For two stars, BAT99-101/102 and BAT99-116, the background-subtracted count number is large enough to render possible the analysis of their X-ray spectra. The spectral analysis has been performed adopting a single-temperature MEKAL optically thin plasma emission model (Kaastra & Mewe 1993; Liedahl et al. 1995), and the photoelectric absorption model of Balucinska-Church & McCammon (1992) for the absorption along the line of sight. The chemical abundances of the X-ray-emitting gas and for the absorbing material have been set to 0.33 Z_{\odot} . The best spectral fits indicate plasma temperatures of 0.9 ± 0.2 and $5.0^{+1.5}_{-1.0}$ keV and hydrogen column densities of $(9 \pm 2) \times 10^{21}$ and $(9 \pm 2) \times 10^{21}$ cm⁻² for BAT99-101/102 and BAT99-116, respectively. Further details of these spectral fits are provided by Guerrero & Chu (2006). The X-ray luminosities in the 0.5–7.0 keV energy band of BAT99-101/102 and BAT99-116 derived from these spectral fits are listed in Table 13. For the other 13 WNL stars detected in X-rays, their X-ray luminosities listed in Table 13 have been derived from their count rate, assuming that their X-ray emission follows a single-temperature MEKAL optically thin plasma emission model with a temperature of 1.6 keV and a hydrogen column density of 3×10^{21} cm⁻² (Guerrero & Chu 2006).

For the WNL stars undetected by *Chandra* and *ROSAT* observations, we have derived count rate 3σ upper limits (see Table 13) using source regions with radii matching the PSF of each observation. These limits assume the same single-temperature MEKAL optically thin plasma emission model as above.

4.8.1 X-Rays and Binarity

As can be seen from Table 13, *Chandra* ACIS is more sensitive than *ROSAT*'s instruments; the latter does not yield a single detection of our program stars. We will therefore concentrate on the *Chandra* data for most of our discussion.

Chandra observed 25 of our 41 program stars, detecting 15 sources. WR+O binaries are expected to be bright X-ray sources because of the high-energy wind-wind collisions

⁸ The Digitized Sky Survey (DSS) is based on photographic data obtained using the UK Schmidt Telescope and the Oschin Schmidt Telescope on Palomar Mountain. The UK Schmidt was operated by the Royal Observatory of Edinburgh, with funding from the UK Science and Engineering Research Council, until 1988 June, and thereafter by the Anglo-Australian Observatory. The Palomar Observatory Sky Survey was funded by the National Geographic Society. The Oschin Schmidt Telescope is operated by the California Institute of Technology and Palomar Observatory. The plates were processed into the present compressed digital form with the permission of these institutes. The Digitized Sky Survey was produced at the Space Telescope Science Institute under US government grant NAGW-2166.

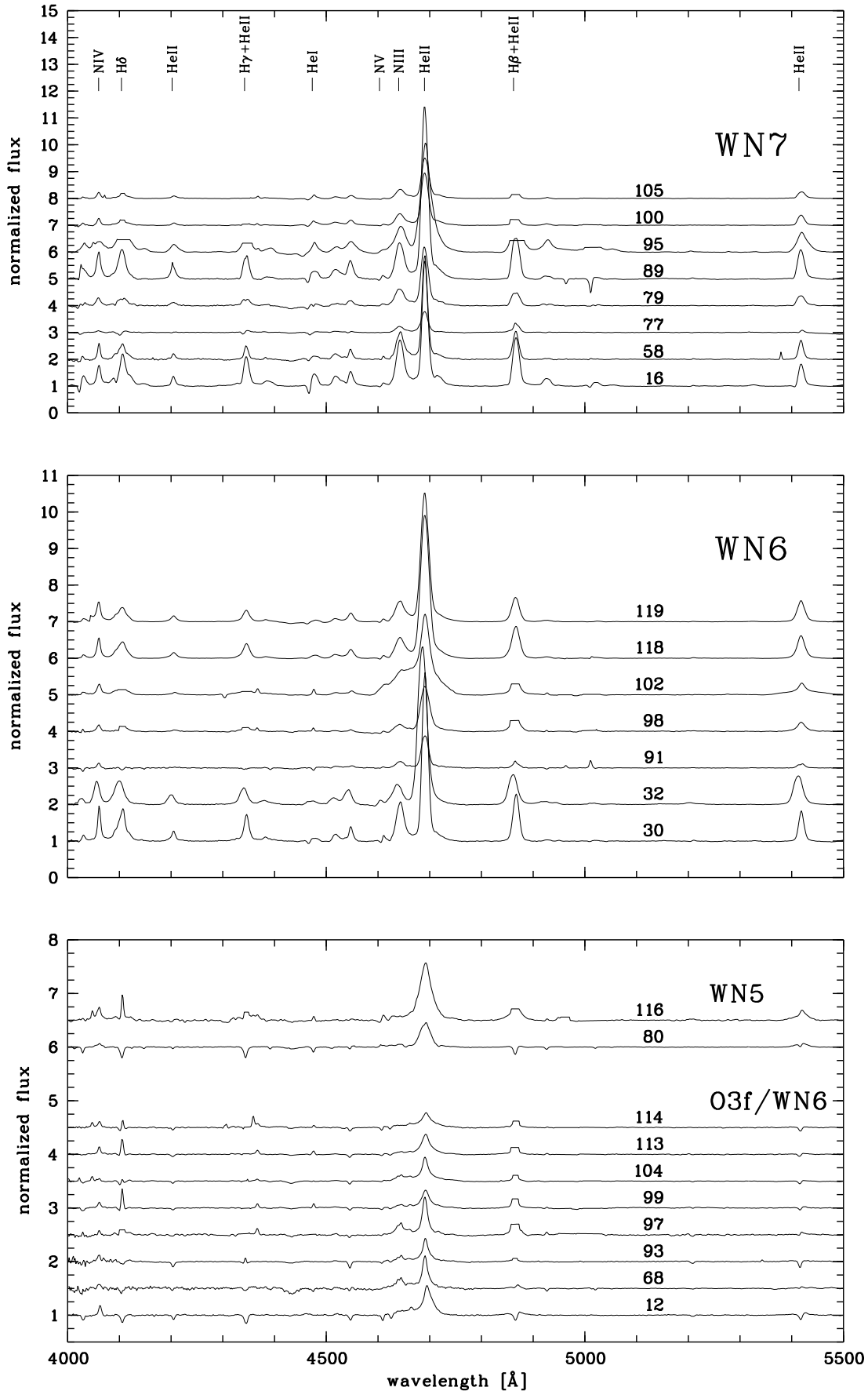


Figure 9. Montages of mean spectra of our program stars. For clarity, spectra have been shifted in flux. Note the different flux scales in each plot. BAT99 numbers are indicated and important emission lines identified.

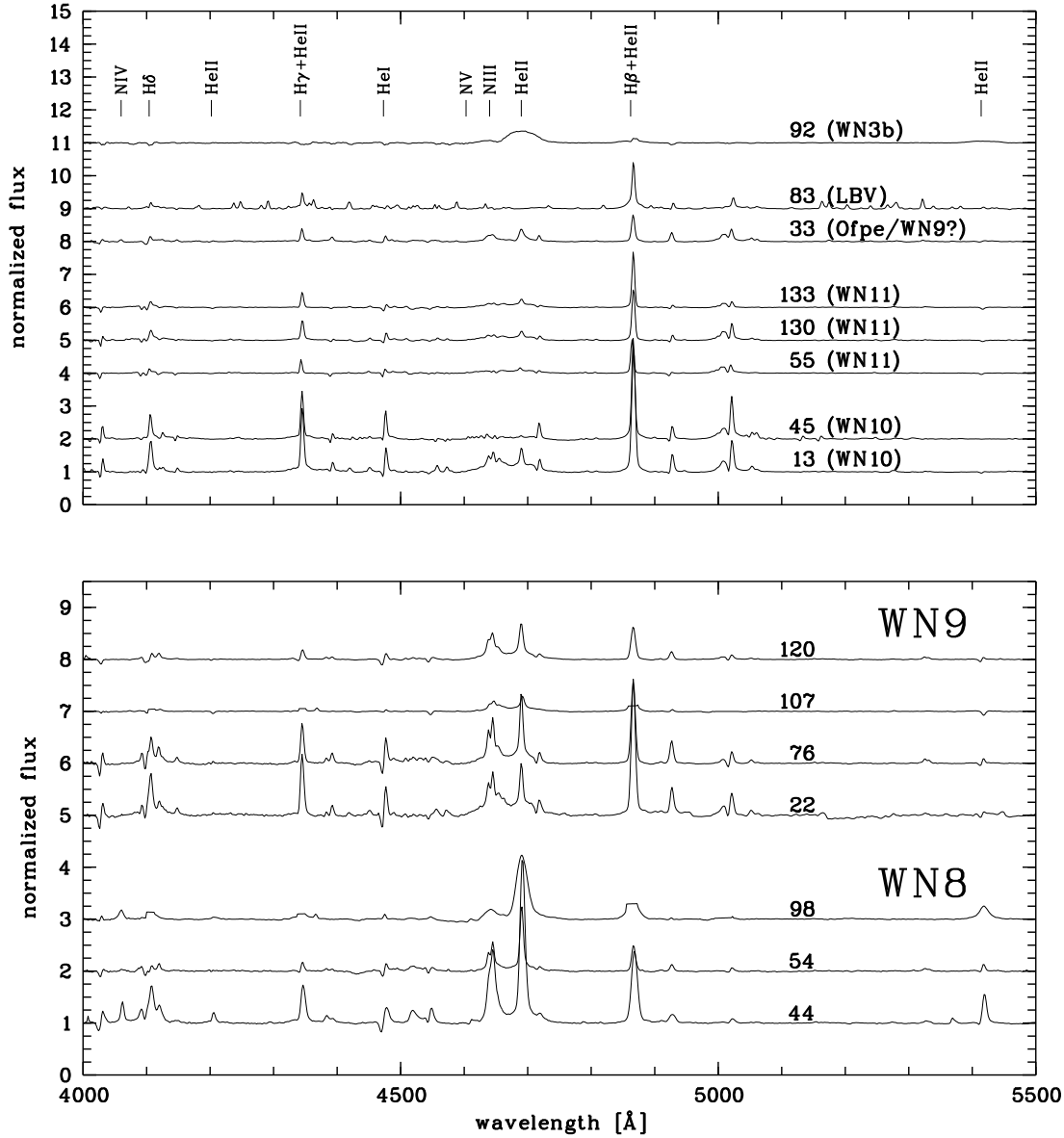


Figure 9 – continued

(WWCs) occurring in such systems (e.g. Prilutskii & Usov 1976). Indeed, phase-dependent profile variations of the $\text{HeII}\lambda 4686$ emission line are readily observed in our binaries (not shown here, but see Foellmi et al. 2003b and Bartzakos et al. 2001). However, of the seven binaries observed, only five are detected, two of which, BAT99-99 and 119, are long-period binaries. Two binary systems, BAT99-95 and 113, were missed, with BAT99-95 apparently being a particularly faint X-ray source. One might suspect that short-period, close binary systems produce fewer observable X-rays, because the two winds have not yet reached their respective terminal velocities, and/or the self-absorption in the wind of generated X-ray photons might decrease the observable flux (see e.g. Owocki & Cohen 2001; Ignace & Gayley 2002). Longer-period binaries, on the other hand, have larger orbital separations, so their winds are potentially faster and geometrically thinned, possibly decreasing self-absorption of the X-rays and resulting in larger observed X-ray fluxes. Along the same lines, one might also ex-

pect that binaries containing hydrogen-depleted WNb stars generate more X-rays because due to their higher mass-loss rates and faster winds, there is more wind momentum available.

In order to test these speculations, we combined our data with those of Foellmi et al. (2003b) and plotted the observed X-ray flux *versus* the orbital period (Figure 10). Non-detections of both *Chandra* and *ROSAT* are given with their upper limit, by downward-pointing arrows. As can be seen, there is no readily apparent trend in the data which could support that longer-period or WNb binaries indeed do display larger X-ray fluxes than shorter-period systems or such which contain WR stars with lower mass-loss rates. However, more data might help to clarify the situation.

Interestingly, BAT99-99 is X-ray brighter than BAT99-119, but this could be due in part to the large eccentricity ($e \sim 0.7$; Schnurr et al., in preparation) of BAT99-119. It is thus not unlikely that *Chandra* missed the moment of maximum X-ray luminosity for BAT99-119 during perias-

Table 13. List of our program stars for which X-ray data are available from public archives.

BAT99	Instrument	Detection?	Count Number [cnts]	Count rate or 3σ upper limit [cnts/s]	L_x or 3σ upper limit [ergs/s]	Comments
12	ROSAT PSPC	No		$< 1.1 \times 10^{-3}$	$< 6.0 \times 10^{33}$	binary(?)
13	ROSAT PSPC	No		$< 4.0 \times 10^{-4}$	$< 2.2 \times 10^{33}$	
16	ROSAT PSPC	No		$< 1.2 \times 10^{-3}$	$< 6.6 \times 10^{33}$	
22	ROSAT PSPC	No		$< 6.8 \times 10^{-4}$	$< 3.7 \times 10^{33}$	
30	ROSAT PSPC	No		$< 3.5 \times 10^{-4}$	$< 1.9 \times 10^{33}$	
32	ROSAT PSPC	No		$< 5.5 \times 10^{-4}$	$< 3.0 \times 10^{33}$	binary
33	ROSAT HRI	No		$< 3.2 \times 10^{-4}$	$< 4.5 \times 10^{33}$	
44	ROSAT PSPC	No		$< 4.3 \times 10^{-4}$	$< 1.6 \times 10^{33}$	
45	ROSAT PSPC	No		$< 3.3 \times 10^{-4}$	$< 1.8 \times 10^{33}$	
54	ROSAT PSPC	No		$< 2.7 \times 10^{-4}$	$< 1.5 \times 10^{33}$	
55	ROSAT PSPC	No		$< 2.8 \times 10^{-4}$	$< 1.5 \times 10^{33}$	
58	ROSAT PSPC	No		$< 1.0 \times 10^{-3}$	$< 5.5 \times 10^{33}$	
68	ROSAT HRI	No		$< 1.9 \times 10^{-4}$	$< 2.7 \times 10^{33}$	
76	ROSAT PSPC	No		$< 2.9 \times 10^{-4}$	$< 1.6 \times 10^{33}$	
77	Chandra ACIS	Yes	18 ± 7	3.1×10^{-4}	$(5 \pm 2) \times 10^{32}$	binary
79	Chandra ACIS	Yes	19 ± 7	3.1×10^{-4}	$(5 \pm 2) \times 10^{32}$	constant RV
80	Chandra ACIS	Yes	45 ± 9	4.9×10^{-4}	$(1.0 \pm 0.2) \times 10^{33}$	constant RV
83	Chandra ACIS	No		$< 1.3 \times 10^{-4}$	$< 2.6 \times 10^{32}$	
89	Chandra ACIS	No		$< 3.7 \times 10^{-4}$	$< 7.4 \times 10^{32}$	
91	Chandra ACIS	No		$< 5.0 \times 10^{-4}$	$< 7.9 \times 10^{32}$	
92	Chandra ACIS	Yes	12 ± 4	6.7×10^{-4}	$(1.3 \pm 0.4) \times 10^{33}$	binary
93	Chandra ACIS	Yes	24 ± 9	5.0×10^{-4}	$(8 \pm 3) \times 10^{32}$	constant RV
95	Chandra ACIS	No		$< 3.2 \times 10^{-4}$	$< 6.4 \times 10^{32}$	binary
96	Chandra ACIS	No		$< 3.5 \times 10^{-4}$	$< 7.0 \times 10^{32}$	
97	Chandra ACIS	No		$< 3.1 \times 10^{-4}$	$< 6.2 \times 10^{32}$	
98	Chandra ACIS	No		$< 3.6 \times 10^{-4}$	$< 7.2 \times 10^{32}$	
99	Chandra ACIS	Yes	77 ± 9	4.4×10^{-3}	$(1.3 \pm 0.2) \times 10^{34}$	binary
100	Chandra ACIS	Yes	8 ± 3	4.1×10^{-4}	$(8 \pm 3) \times 10^{32}$	constant RV
101,102	Chandra ACIS	Yes	330 ± 20	1.9×10^{-2}	$(1.5 \pm 0.1) \times 10^{35}$	slightly variable RV
103	Chandra ACIS	Yes	7 ± 3	3.8×10^{-4}	$(8 \pm 3) \times 10^{32}$	binary
104	Chandra ACIS	No		$< 5.1 \times 10^{-4}$	$< 1.0 \times 10^{33}$	
105	Chandra ACIS	Yes	21 ± 5	1.2×10^{-3}	$(2.4 \pm 0.6) \times 10^{33}$	variable RV
107	Chandra ACIS	Yes	16 ± 4	9.2×10^{-4}	$(1.8 \pm 0.5) \times 10^{33}$	slightly variable RV
113	Chandra ACIS	No		$< 6.4 \times 10^{-4}$	$< 1.3 \times 10^{33}$	binary
114	Chandra ACIS	Yes	9 ± 3	5.1×10^{-4}	$(1.0 \pm 0.3) \times 10^{33}$	slightly variable RV
116	Chandra ACIS	Yes	860 ± 30	4.9×10^{-2}	$(1.8 \pm 0.1) \times 10^{35}$	variable RV
118	Chandra ACIS	Yes	13 ± 4	7.5×10^{-4}	$(1.5 \pm 0.5) \times 10^{33}$	variable RV
119	Chandra ACIS	Yes	11 ± 4	6.1×10^{-4}	$(1.2 \pm 0.4) \times 10^{33}$	binary
120	Chandra ACIS	No		$< 3.6 \times 10^{-3}$	$< 5.7 \times 10^{33}$	
130	ROSAT HRI	No		$< 7.0 \times 10^{-4}$	$< 1.0 \times 10^{34}$	
133	ROSAT PSPC	No		$< 7.1 \times 10^{-3}$	$< 3.9 \times 10^{34}$	

tron passage. Note however that the circular orbit which was assumed for BAT99-99 might be incorrect, and that this binary is eccentric, too. In fact, both systems merit a closer look for orbit-related X-ray variability.

4.8.2 X-Rays in Apparently Single Stars

Of the remaining 10 stars detected by *Chandra*, four have X-ray luminosities which are comparable to those of the confirmed binaries although they do not show RV variability: BAT99-79, 80, 93, 100. Six do display RV variability: BAT99-101/102, 105, 107, 114, 116, and 118. Crowding might account for the recorded high X-ray fluxes, and there still is the possibility that the X-rays originate in single WR stars due to radiatively-induced instabilities in their winds (Lucy & White 1980; Willis & Stevens 1996). It can

however not be ruled out that these stars are long-period ($P > 200$ days) binaries or systems with very low inclination angles.

Two detected sources, BAT99-101/102 and 116, are extremely luminous. BAT99-101/102 are two visually very close stars, and thus *Chandra*'s aperture integrated the combined flux. BAT99-101 is a WC4 star (Bartzakos et al. 2001) and potentially a binary (Bartzakos et al. 2001), while for BAT99-102, there is some confusion: As detailed above, we find that BAT99-103 is the 2.76-day binary, not 102, as was reported by Moffat (1989). However, even if 102 is single, there might be sufficient wind momentum confined in a very small volume, and if both 101 and 102 are binary, then there most certainly is enough WWC occurring to account for the observed X-ray flux.

BAT99-116, on the other hand, is visually isolated enough not to be subject to such ambiguities. BAT99-116

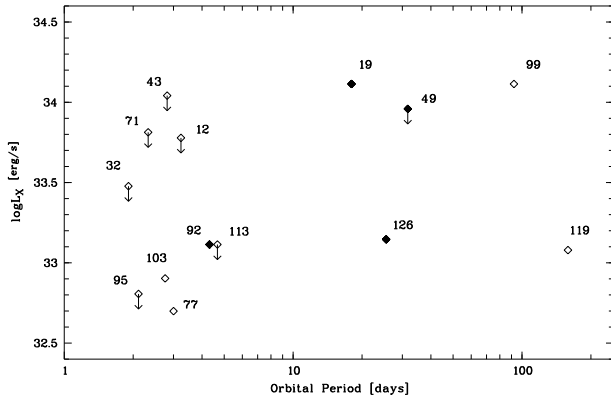


Figure 10. X-ray luminosities of identified WN binaries in the LMC as a function of their orbital period. Filled symbols denote broad-lined, hydrogen-depleted WNb stars; empty symbols denote H-containing WN stars. Upper limits are indicated by downward-pointing arrows, and stars are named by their BAT99 numbers. As can be seen, WNb binaries do not show higher X-ray luminosities as might have been expected from the stronger winds of WNb stars.

is even more X-ray luminous than the combined BAT99-101/102 system, and comparable to the X-ray brightest WR stars known, the Galactic WN6ha stars NGC3603-C (Moffat et al. 2002) and WR25 (Seward & Chlebowski 1982). Both NGC3603-C (Schnurr et al., in prep.) and WR25 (Gamen et al. 2006) have been identified as binaries, and they both contain two of the most luminous WN stars known, so that there is a plausible explanation as to why these objects are so X-ray bright. However, although 116 displays significant RV variability (Section 4.3), no indication of binarity could be found. Unless the photometry published by BAT99 is wrong, 116 is not particularly optically bright, either, ~ 1.5 mag fainter than BAT99-119, which is a confirmed binary. Since both stars are similar enough (WN5ha for 116, and WN6ha for 119; see above) to have the \sim -same bolometric correction (no reddening considered, but it is low and probably \sim -similar for the two stars anyway), 116 is considerably less luminous and hence less massive than 119. Thus, if 116 is indeed single, its ratio L_x/L_{bol} is abnormally high, but if X-rays originate from WWCs in a binary, the question remains how such faint objects (the total mass has now to be split between two stars) can provide the required wind momenta. This very intriguing system merits a closer look.

As to BAT99-118, the sheer bolometric luminosity of the object (Crowther & Dessart 1998) renders a two-star scenario more likely. BAT99-118 closely resembles 119 in terms of both spectral type and X-ray luminosity (the latter is, in fact, equal within the errors). It is thus possible that BAT99-118 will turn out to be a long-period binary as well, especially given the fact that it also shows a significantly large RV scatter.

5 DISCUSSION

5.1 Binary Detectability and Completeness

Before we can discuss the binary frequency among WNL stars in the LMC, we have to address the question of how many binaries we missed. To do so, let us consider some general aspects of binary detection. Most approaches dealing with how to detect a binary through RV variations are based on statistical tests which compare the observed RV scatter σ_{RV} of a binary candidate to the (Gaussian) scatter of an observed, constant comparison star (via a χ^2 test), just as we have done in Sec. 4.3. How large does the RV amplitude of a given binary have to be so that it can be identified as a RV-variable star? The RV amplitude K_{RV} of the WR is given by

$$K_{WR} = 212.7 M_{\odot} / (M_{WR} + M_{\odot})^{2/3} P^{-1/3} (1 - e^2)^{-1/2} \sin i,$$

where K_1 is in kms^{-1} , all masses in M_{\odot} , and P in days. For a circular orbit ($e = 0$) and *continuous* sampling, the RV scatter is $\sigma_{RV} = K/\sqrt{2}$, and it has to be larger than some detection threshold σ_{cut} for the star to be considered as significantly variable. In Section 4.3, we defined the 99.9%ile to be $\sigma_{cut} = 22.6 \text{ kms}^{-1}$.

As already mentioned, some very luminous stars in our sample, such as the WN5-7ha and O3f/WN6 stars, are not evolved, classical, He-burning WN stars, but unevolved, very massive objects; when situated in binary systems, they usually are (much) more massive than their companion, while classical, evolved WN stars usually are the less massive component. To cover the range of possible mass ratios, we have thus fixed the mass of the O-type component to $40 M_{\odot}$ and computed the σ_{RV} 's for two different masses of the WN component, $80 M_{\odot}$ (for the unevolved case) and $20 M_{\odot}$ (for the evolved case), and for two different inclination angles, $i = 90^\circ$ and $i = 30^\circ$, assuming circular orbits. Values of σ_{RV} are plotted versus the binary period P in Figure 11.

It can clearly be seen that all binaries are well above our detection threshold, and that we should in principle be able to see evolved WN stars with periods somewhat longer than 100 days. In particular, there is no reason why we should not be able to see systems with periods between 5 and 90 days, of which there is an apparent lack in our study. To miss these systems, their inclination angles would have to be extremely low. However, as Foellmi et al. (2003a) have shown, in a sample with randomly distributed inclination angles there are 6.5 times more binaries between 90° and 30° than there are between 30° and 0° ; thus, it is very unlikely that there is a significant number of low-inclination systems in our sample, in particular if these harbour evolved (i.e., lower-mass) WN stars, which are the primary focus of our study.

Let us further note that, while from our RV data alone, we were not able to detect the binary nature of BAT99-119, because its period of ~ 160 days is too long and its orbit is too eccentric, we did detect its large RV scatter, which firmly puts it above our variability threshold. We were also able to identify BAT99-99's period of ~ 92 days and even obtain an orbital solution (albeit a preliminary one), despite the fact that this O3f*/WN6 star is an unevolved object, too, and thus more massive than its companion.

Thus, we can be quite confident that systems with periods between 5 and 90 days are indeed absent in our program

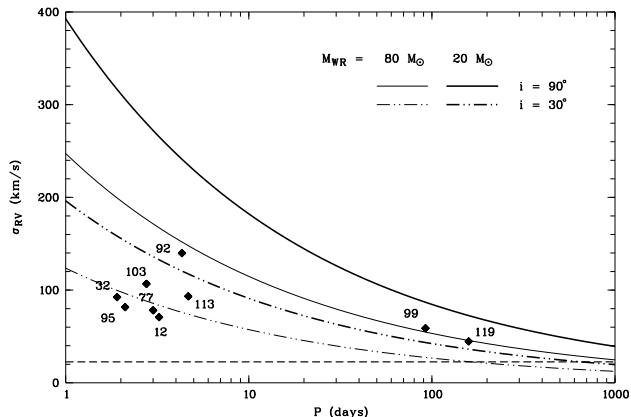


Figure 11. Curves show RV scatter $\sigma_{RV} = K/\sqrt{2}$ for the WN component in two fictitious, continuously sampled, circular binaries, computed for periods ranging from 1 to 1000 days. The mass of the O-type secondary is fixed at $40 M_{\odot}$, while the mass of the WN component is $80 M_{\odot}$ (thin lines) or $20 M_{\odot}$ (thick lines), to represent the unevolved and the evolved cases. Solid lines indicate $i = 90^{\circ}$, whereas dash-dotted lines are for $i = 30^{\circ}$. The dashed, horizontal line indicates the 99.9% detection threshold of our χ^2 test. Identified WNL binaries with both their observed RV scatter and their BAT99 numbers are given. For BAT99-119, we have used the period reported by Schnurr et al. (in preparation).

stars, and that we are quite complete for evolved WN binaries with periods up to 200 days. Of course, this estimate of our detection limits is very rough, because elliptical orbits and discrete sampling will modify the individual detection limit of a binary system. Since we have also searched for periodicities in our RV data, the problem of binary detection is shifted into the realm of Fourier statistics. (Note, however, that cyclical variability in the RV data is a necessary, but not a sufficient condition for binarity, because rotation or pulsation could induce a periodically variable RV pattern.) In this case, the whole situation becomes more intricate, since not only the total time span T covered by observations compared to the systemic periods P becomes important, but also the distribution of data points in phase. Detection limits do not directly depend on the ratio of the RV amplitude K of the primary star (the signal) to the measurement error σ (the noise) in data space, but on the S/N ratio achieved in the frequency domain.

At a given number of data points covering a certain time span, short periods generally have a large T/P and better “phase-filling”, and therefore have a larger detection probability than longer periods which suffer from holes in the phase coverage and a lower S/N per frequency unit. Vice versa, the same detection probability as for longer periods can be obtained for shorter periods but lower RV amplitudes, which means that low- K (low-inclination) binaries with a given K tend to be detected more easily if they are short-period.

In the case of non-circular orbits, the eccentricity, the orientation of the orbital ellipse, and the time of periastron passage seriously affect the detection probability of periods for two reasons. First, the orbital RV curve becomes distorted in a way that generates harmonics in the Fourier spectrum. Power is transferred from the fundamental to the

harmonics, thereby lowering the peak of the fundamental frequency. If the orbit is highly eccentric, the fundamental peak might be pushed into the noise floor, and the period will not be detected. Second, the distribution of the data points over the orbital phase is even more critical, because the star spends most of the time near apastron; if the passage of periastron, where the RVs change rapidly, is missed, the RV curve will look flatter than it really is. This is a problem for any σ_{RV} -based statistics in velocity space, because it is possible that observed RVs display cyclical variability in the sense that a period has been found, although the observed RV scatter is *not* significantly large.

The standard approach to deal with this problem is a Monte-Carlo simulation of a population of artificial binaries by randomly drawing orbital parameters following a pre-determined distribution function, and applying the desired test statistics in RV and/or frequency space, or by actually full Keplerian fitting; for reasons of convenience and computational expense, usually only the former is done. From the detected fraction of artificial binaries, one can reconstruct the true binary frequency among the artificial sample by statistical means. (For an excellent description of this approach and all related problems, see Kouwenhoven 2006).

The main problem, however, is to determine reasonable distribution functions for the respective orbital parameters, because the results of the simulation will obviously depend strongly on what initial assumptions were made for the underlying, true binary population. For their WNE stars in the LMC, Foellmi et al. (2003b) used distribution functions for Galactic O stars (based on statistics published by Mason et al. 1998; also see references therein); they found that 35% of the binaries in their sample were missed. For our study, the most relevant assumption Foellmi et al. used was that the orbital periods P are distributed flat in $\log P$, i.e. there are as many binaries between 1 and 10 days as there are between 10 and 100 days, etc. In our WNL sample, we have found eight binaries with periods shorter than 100 days. Of these eight binaries, only one, BAT99-99, has a period between 10 and 100 days; the remaining seven binaries have periods ranging between 1 and 10 days. Thus, without any sophisticated Monte Carlo simulation, we can immediately determine that we would have missed six binaries in the period range from 10 to 100 days, but of course only if we believed that we are complete in the period range from 1 to 10 days and that our chosen period distribution is correct.

But how sound is this assumption? Indeed, the distribution function for pre(!)-RLOF, O+O binary periods is not suited for statistics of post-RLOF populations, when one of the model predictions is that orbital periods change due to binary interaction. Clearly, however, any other choice of distribution function would produce a different result. Moreover, our analysis above indicates that it is unlikely that we missed binaries between 5 and 90 days, and of course one must not forget that we operate with small numbers. Thus, even if we had a way to obtain the true number of expected binaries from the number of observed binaries, we would have to show first that the observed number is statistically not consistent with the expected value; otherwise, any correction would not be justified. Because of those severe imponderabilities, we not carry out any statistical correction, but consider the number of binaries that we have found

Table 14. Known binaries among the WNL population of the LMC, where the O3f*/WN6A stars have been counted in. The improved period for BAT99-119 was taken from Schnurr et al. (in prep).

BAT99	Period [days]	Spectral Type (this study)	Comments
12	3.24	O3f*/WN6A	new
32	1.91	WN6(h)	
77	3.00	WN7ha	
95	2.11	WN7	new
99	92.60	O3f*/WN6-A	new
103	2.76	WN6	
113	4.70	O3f*/WN6-A	new
119	158.80	WN6(h)	

as a lower limit only. We will also consider that, whatever the detection bias is, Bartzakos et al. (2001), Foellmi et al. (2003b), and this study suffer from it in roughly the same way, given that we have carried out more or less the same kind of observations. In regard to the achieved RV precision, one can argue that the somewhat better precision obtained in this study is compensated by the fact that classical WNL stars are expected to be, on average, more massive than WNE and WC/WO stars, because they had less time to shed mass by stellar winds; thus, RV amplitudes of WNL binaries will, on average, be somewhat smaller than those of WNE and WC/WO binaries. Since neither of the three studies used a more sophisticated detection threshold than the RV scatter of (presumably) constant, reference stars, we feel that all three studies have \sim the same detection probability for periods up to ~ 200 days. Thus, we consider the three studies to be directly comparable.

5.2 The Binary Frequency among the WNL Stars in the LMC

The present survey encompassed all 41 WNL stars listed in the BAT99 catalogue outside R136. The remaining 6 WNL stars in the core of R136 required higher spatial resolution, e.g. adaptive-optics assisted spectroscopy with VLT/SINFONI; the work is in progress and results will be published elsewhere (Schnurr et al., in preparation), but preliminary results indicate that there is no short-period ($P \lesssim 20$ days) binary among those stars. Foellmi et al. (2003b) reclassified one of their program stars, BAT99-78, to WN6 (i.e. to WNL); in turn, one of our stars, BAT99-92, was recognized to be an early-type WN3b star (cf. Section 4.7). Thus, the respective numbers of WNE and WNL stars which have been studied remain unchanged: There are 47 WNL stars in the LMC.

In this study, we are only interested in binaries with periods up to ~ 200 days. A binary counts as detected only if an orbital solution could be established. Using this criterion, eight stars have been recognized as binaries (cf. Table 14): BAT99-12, 32, 77, 92, 95, 99, 103, 113. By combining our RV data with those of Moffat (1989) and with unpublished polarimetry, a ninth binary, BAT99-119, was identified (Schnurr et al., in preparation). Moffat (1989) reported 6 binaries among the 14 WNL stars he had studied. Our study has added four previously unknown WNL

Table 15. Spectroscopic binary frequencies for three different subgroups in the LMC.

Subgroup	Frequency	References
WNL	8/ 41 = 0.20	this study
WNE	8/ 61 = 0.13	Foellmi et al. (2003b)
WNL+WNE	16/102 = 0.15	
WC+WO	3/ 24 = 0.13	Bartzakos et al. (2001)
WR all	19/126 = 0.15	

binary systems to that list, and confirmed four known binaries and their orbital periods. One of Moffat’s (1989) binaries, BAT99-107, was however found to be a single star. From significantly large RV scatter, visual brightness or high X-ray luminosity, two additional stars, BAT99-116 and 118, qualify as binary candidates in the period-range of interest (i.e. up to 200 days), while more stars might be binaries with (considerably) longer periods than that. With BAT99-32 being a WNE binary, the confirmed WNL binary frequency is $8/41 = 20\%$.

Interestingly, no binaries or RV variables can be found among the WN8,9 stars in our sample – as a matter of fact, they yield the smallest RV scatter of our sample stars –, whereas WN6,7 stars do show binaries among them. This seems to confirm the findings of Moffat (1989), who suspected that this dichotomy reflected deeper differences between WN6,7 and WN8,9 stars. He argued that Galactic WN8,9 stars tended to be single runaways (an observation that we cannot confirm from the systemic velocities measured for our WN8,9 stars in our sample), and that in the LMC, WN8,9 stars tend to avoid clusters, very much unlike WN6,7 star. While since Moffat (1989), the spectral type of the Galactic binary WR12 (Rauw et al. 1996) was revised from WN7 to WN8 by Smith et al. (1996), Moffat’s (1989) conclusion still holds.

5.3 Comparison with WNE and WC/WO stars

Among the 61 WNE stars in the LMC, Foellmi et al. (2003b) reported only five certain binaries, two systems with unreliable orbital solutions (which we count as identified), and two potential binaries; we have added to this BAT99-92, so that the confirmed binary frequency among the WNE stars in the LMC is now $8/61 = 13\%$. If one combines the results for WNE and WNL stars, one obtains 102 WN stars studied among which $8 + 8 = 16$ are confirmed binaries; thus, the confirmed binary frequency is $16/102 = 15\%$. Among the 24 WC/WO stars, Bartzakos et al. (2001) studied 23 and reported three confirmed binaries. The 24th star is very faint and thus likely single. While they also reported 5 potential binaries, even the one with the largest RV scatter, MG6, failed to be significantly (99% confidence level) variable; therefore, we consider their remaining binary candidates to be constant as well. This brings the binary frequency among 24 WC/WO stars in the LMC to 3; thus, the binary frequency is $3/24 = 13\%$. Values are quoted in Table 15. Note that the binary frequencies among the different subgroups (WNL, WNE, and WC/WO) are statistically fully consistent with each other.

6 SUMMARY AND CONCLUSION

We have carried out spectroscopic monitoring of all 41 WNL stars in the LMC that could be observed by conventional, ground-based observations. Measured RV curves were used to identify binaries with orbital periods from 1 to ~ 200 days, because these systems were expected to be post-RLOF candidates (cf Vanbeveren et al. 1998). Additionally, publicly available archive data from X-ray satellite missions were searched for our program stars to obtain X-ray luminosities. The results of our study can be summarized as follows (see also Table 14):

- We have identified four previously unknown binary systems: BAT99-12, 95, 99, and 113.
- We confirmed the previously known binaries BAT99-32, 77, 92. However, while we could reproduce the 2.76-day period that Moffat (1989) had reported for star BAT99-102, we did so for star BAT99-103. It presently remains unknown whether Moffat (1989) or we wrongly identified the binary.
- We also confirmed that BAT99-119 is a binary; however, we had to combine our RV data with those of Moffat (1989) to do so, and it required further combination with previously unpublished polarimetry to identify the 159-day period of the system. For reasons of completeness, we list the results here, but the complete study will be published elsewhere (Schnurr et al., in prep).
- One star, BAT99-107, had been suspected binary by Moffat (1989), but we were unable to reproduce that results. Therefore, we consider 105 to be single (i.e., not a binary with an orbital period in the quoted range).
- Two binary candidates were identified from their RV variability and their X-ray luminosities, BAT99-116 and 118. Both systems merit a closer look, because 116 is one of the brightest X-ray sources among all WR stars, while 118 is the most luminous WR star and thus, the most luminous unevolved star known in the Local Group (cf. Crowther & Dessart 1998).
- One of our program stars, BAT99-92, a binary, was recognized to be a WNE and not a WNL star.
- Thus, our study brings the total number of known WNL binaries to 8, and the binary frequency among WNL stars in the LMC to 20%, which is fully consistent with the results for WC/WO stars (Bartzakos et al. 2001) and WNE stars (Foellmi et al. 2003b); thus, there is no statistically significant differences between different WR populations in the LMC. However, the overall binary frequency is only half of what was predicted from model results by Maeder & Meynet (1994). The implications of this low binary frequency for massive-star evolution will be discussed in a forthcoming paper.

Remarkably, none of the WNL binaries contains a classical, hydrogen-deficient, helium-burning WR star; instead, the WN components are young, unevolved, objects (hot O3If/WN6 stars or more extreme WN5-7ha stars), which most likely are very luminous and hence very massive Of stars, and possibly even the most massive stars known. These binaries offer the tremendous opportunity to directly weigh these extreme stars using model-independent, Keplerian orbits. Follow-up observations have partly been obtained and are currently reduced, or are under way. The results of these observations will be published elsewhere.

ACKNOWLEDGMENTS

OS is grateful to the various TACs for the generous allocation of telescope time and for the very warm hospitality at all involved observatories, as well as the quick, uncomplicated and competent help of the night assistants, telescope operators, and observatory staff in all situations. OS particularly thanks Stéphane Vennes for introduction at the Mount Stromlo 74-in telescope and his help during the observing runs, and Marilena Salvo for introduction at the Siding Spring 2.3-m telescope. OS also thanks the Mount Stromlo administration for uncomplicated re-scheduling at Siding Spring after the 74-in telescope at Stromlo was lost in the January 18, 2003 bushfires. OS is grateful to Cédric Foellmi for having provided data of the WNE stars, to André-Nicolas Chené for help and very fruitful discussions, and to Paul Crowther for comments that led to improvement of this manuscript. AFJM and NSL are grateful for financial aid from the Natural Sciences and Engineering Council (NSERC) of Canada.

REFERENCES

- Auer L. H., van Blerkom D., 1972, *ApJ*, 178, 175
 Balucinska-Church M., McCammon D., 1992, *ApJ*, 400, 699
 Bartzakos P., Moffat A. F. J., Niemela V. S., 2001, *MNRAS*, 324, 18
 Blaauw A., 1961, *BAN*, 15, 265
 Bonanos A. Z., Stanek K. Z., Udalski A., Wyrzykowski L., Żebruń K., Kubiak M., Szymański M. K., Szweczyk O., Pietrzyński G., Soszyński I., 2004, *ApJ*, 611, L33
 Breysacher J., Azzopardi M., Testor G., 1999, *A&AS*, 137, 117
 Conti P. S., 1976, *Mem. Soc. Roy. Sc. de Liège*, 9, 193
 Crowther P. A., Bohannan B., 1997, *A&A*, 317, 532
 Crowther P. A., Dessart L., 1998, *MNRAS*, 296, 622
 Crowther P. A., Smith L. J., 1997, *A&A*, 320, 500
 Crowther P. A., Smith L. J., Hillier D. J., 1995, *A&A*, 302, 457
 Foellmi C., 2004, *A&A*, 416, 291
 Foellmi C., Moffat A. F. J., Guerrero M. A., 2003a, *MNRAS*, 338, 360
 Foellmi C., Moffat A. F. J., Guerrero M. A., 2003b, *MNRAS*, 338, 1025
 Gamen R., Gosset E., Morrell N., Niemela V., Sana H., Nazé Y., Rauw G., Barbá R., Solivella G., 2006, *A&A*, 460, 777
 Guerrero M. A., Chu Y.-H., 2006, *ApJS*, submitted
 Hillier D. J., 1989, *ApJ*, 347, 392
 Humphreys R. M., Davidson K., 1979, *ApJ*, 232, 409
 Humphreys R. M., Davidson K., 1994, *PASP*, 106, 1025
 Ignace R., Gayley K. G., 2002, *ApJ*, 568, 954
 Kaastra J. S., Mewe R., 1993, *A&AS*, 97, 443
 Kaufer A., Stahl O., Wolf B., Gaeng T., Gummertsbach C. A., Kovacs J., Mandel H., Szeifert T., 1996, *A&A*, 305, 887
 Keller S. C., Wood P. R., 2006, *ApJ*, 642, 834
 Kim S., Staveley-Smith L., Dopita M. A., Freeman K. C., Sault R. J., Kesteven M. J., McConnell D., 1998, *ApJ*, 503, 674

- Kippenhahn R., Weigert A., 1967, *zast*, 65, 251
- Kouwenhoven M. B. N., 2006, ArXiv Astrophysics e-prints
- Kreyszig E., 1975, *Statistische Methoden und ihre Anwendungen*. Göttingen: Vandenhoeck & Ruprecht
- Lamers H. J. G. L. M., Maeder A., Schmutz W., Cassinelli J. P., 1991, *ApJ*, 368, 538
- Liedahl D. A., Osterheld A. L., Goldstein W. H., 1995, *ApJ*, 438, L115
- Lomb N. R., 1976, *Ap&SS*, 39, 447
- Lucy L. B., White R. L., 1980, *ApJ*, 241, 300
- Maeder A., Conti P. S., 1994, *ARA&A*, 32, 227
- Maeder A., Meynet G., 1994, *A&A*, 287, 803
- Maeder A., Meynet G., 2000, *ARA&A*, 38, 143
- Marchenko S. V., Moffat A. F. J., Koenigsberger G., 1994, *ApJ*, 422, 810
- Mason B. D., Gies D. R., Hartkopf W. I., Bagnuolo Jr. W. G., ten Brummelaar T., McAlister H. A., 1998, *AJ*, 115, 821
- Massey P., Duffy A. S., 2001, *ApJ*, 550, 713
- Massey P., Olsen K. A. G., Parker J. W., 2003, *PASP*, 115, 1265
- Massey P., Puls J., Pauldrach A. W. A., Bresolin F., Kudritzki R. P., Simon T., 2005, *ApJ*, 627, 477
- Moffat A. F. J., 1989, *ApJ*, 347, 373
- Moffat A. F. J., 1991, *A&A*, 244, L9+
- Moffat A. F. J., Corcoran M. F., Stevens I. R., Skalkowski G., Marchenko S. V., Mücke A., Ptak A., Koribalski B. S., Brenneman L., Mushotzky R., Pittard J. M., Pollock A. M. T., Brandner W., 2002, *ApJ*, 573, 191
- Moffat A. F. J., Niemela V. S., Phillips M. M., Chu Y.-H., Seggewiss W., 1987, *ApJ*, 312, 612
- Moffat A. F. J., Seggewiss W., 1986, *ApJ*, 309, 714
- Niemela V. S., Seggewiss W., Moffat A. F. J., 2001, *A&A*, 369, 544
- Nikolaev S., Drake A. J., Keller S. C., Cook K. H., Dalal N., Griest K., Welch D. L., Kanbur S. M., 2004, *ApJ*, 601, 260
- Nota A., Pasquali A., Drissen L., Leitherer C., Robert C., Moffat A. F. J., Schmutz W., 1996, *ApJS*, 102, 383
- Owocki S. P., Cohen D. H., 2001, *ApJ*, 559, 1108
- Paczyński B., 1967, *Acta Astronomica*, 17, 355
- Pasquali A., Langer N., Schmutz W., Leitherer C., Nota A., Hubeny I., Moffat A. F. J., 1997, *ApJ*, 478, 340
- Prilutskii O. F., Usov V. V., 1976, *SvA*, 20, 2
- Rauw G., De Becker M., Nazé Y., Crowther P. A., Gosset E., Sana H., van der Hucht K. A., Vreux J.-M., Williams P. M., 2004, *A&A*, 420, L9
- Rauw G., Vreux J.-M., Gosset E., Hutsemekers D., Magain P., Rochowicz K., 1996, *A&A*, 306, 771
- Rauw G., Vreux J.-M., Gosset E., Manfroid J., Niemela V. S., 1996, in Vreux J. M., Detal A., Fraipont-Caro D., Gosset E., Rauw G., eds, *Liège International Astrophysical Colloquia Vol. 33 of Liège International Astrophysical Colloquia*, A new orbital solution for the WNL binary system WR12. pp 303+
- Roberts D. H., Lehar J., Dreher J. W., 1987, *AJ*, 93, 968
- Scargle J. D., 1982, *ApJ*, 263, 835
- Schwarz U. J., 1978, *A&A*, 65, 345
- Schwarzenberg-Czerny A., 1989, *MNRAS*, 241, 153
- Schweickhardt J., Schmutz W., Stahl O., Szeifert T., Wolf B., 1999, *A&A*, 347, 127
- Selman F. J., Melnick J., 2005, *A&A*, 443, 851
- Seward F. D., Chlebowski T., 1982, *ApJ*, 256, 530
- Smith L. F., Shara M. M., Moffat A. F. J., 1996, *MNRAS*, 281, 163
- Stahl O., 1987, *A&A*, 182, 229
- Stahl O., Wolf B., Klare G., Cassatella A., Krautter J., Persi P., Ferrari-Toniolo M., 1983, *A&A*, 127, 49
- Udalski A., Szymanski M., Kubiak M., Pietrzynski G., Soszynski I., Wozniak P., Zebrun K., 2000, *Acta Astron.*, 50, 307
- Vanbeveren D., Van Rensbergen W., De Loore C., 1998, *The Brightest Binaries. The brightest binaries / by D. Vanbeveren, W. van Rensbergen and C. De Loore*. Boston : Kluwer Academic, 1998.
- Vink J. S., de Koter A., Lamers H. J. G. L. M., 2000, *A&A*, 362, 295
- Vink J. S., de Koter A., Lamers H. J. G. L. M., 2001, *A&A*, 369, 574
- Walborn N. R., 1986, in de Loore C. W. H., Willis A. J., Laskarides P., eds, *Luminous Stars and Associations in Galaxies Vol. 116 of IAU Symp. Proc.*, Optical and ultraviolet spectral morphology of luminous OB stars in the Galaxy and the Magellanic Clouds. pp 185–196
- Walborn N. R., Howarth I. D., Lennon D. J., Massey P., Oey M. S., Moffat A. F. J., Skalkowski G., Morrell N. I., Drissen L., Parker J. W., 2002, *AJ*, 123, 2754
- Wellstein S., Langer N., 1999, *A&A*, 350, 148
- Willis A. J., Stevens I. R., 1996, *A&A*, 310, 577